Bacillus velezensis **HBXN2020 alleviates** ***Salmonella*** **Typhimurium infection in mice by improving intestinal barrier integrity and reducing inflammation**

Linkang Wang,[1,2,3] Haiyan Wang,[1,2,3] Xinxin Li,[1,2,3] Mengyuan Zhu,[1,2,3] Dongyang Gao,[1,2,3] Dayue Hu,[1,2,3] Zhixuan Xiong,[1,2,3] Xiangmin Li[1,2,3]* and Ping Qian[1,2,3]*

[1]*National Key Laboratory of Agricultural Microbiology, Hubei Hongshan Laboratory, Huazhong Agricultural University, Wuhan, Hubei, 430070, People's Republic of China*.

[2]*College of Veterinary Medicine, Huazhong Agricultural University, Wuhan, Hubei, People's Republic of China*.

[3]*Key Laboratory of Preventive Veterinary Medicine in Hubei Province, the Cooperative Innovation Center for Sustainable Pig Production, Wuhan, Hubei, People's Republic of China*.

* Corresponding author: Ping Qian: Tel: 86-27-87282608; Fax: 86-27-87282608; E-mail: qianp@mail.hzau.edu.cn. Address: No. 1, Shizishan Street, Hongshan District, Wuhan City, Hubei Province, China.

* Co-corresponding author: Xiang-min Li: Tel: 86-27-87282608; Fax: 86-27-87282608; E-mail: lixiangmin@mail.hzau.edu.cn. Address: No. 1, Shizishan

Street, Hongshan District, Wuhan City, Hubei Province, China.

Abstract

Bacillus velezensis is a species of *Bacillus* that has been widely investigated because of its broad-spectrum antimicrobial activity. However, most studies on *Bacillus velezensis* have focused on the biocontrol of plant diseases, with few reports on antagonizing *Salmonella* Typhimurium infections. In this investigation, it was discovered that *Bacillus velezensis* HBXN2020, which was isolated from healthy black pigs, possessed strong anti-stress and broad-spectrum antibacterial activity. Importantly, *Bacillus velezensis* HBXN2020 did not cause any adverse side effects in mice when administered at various doses (1×10^7, 1×10^8, and 1×10^9 CFU) for 14 d. Supplementing *Bacillus velezensis* HBXN2020 spores, either as a curative or preventive measure, dramatically reduced the levels of *Salmonella* Typhimurium ATCC14028 in the mice's feces, ileum, cecum, and colon, as well as the disease activity index (DAI), in a model of infection caused by this pathogen in mice. Additionally, supplementing *Bacillus velezensis* HBXN2020 spores significantly regulated cytokine levels (TNF-α, IL-1β, IL-6, and IL-10) and maintained the expression of tight junction proteins and mucin protein. Most importantly, adding *Bacillus velezensis* HBXN2020 spores to the colonic microbiota improved its stability and increased the amount of beneficial bacteria (*Lactobacillus* and *Akkermansia*). All together, *Bacillus velezensis*

HBXN2020 can improve intestinal microbiota stability and barrier integrity and reduce inflammation to help treat infection by *Salmonella* Typhimurium.

Key words: *Bacillus velezensis*; antibacterial activity; *S.* Typhimurium infection; infections; gut health

Introduction

Salmonella Typhimurium (*S.* Typhimurium) is a major foodborne zoonotic pathogen that can cause diarrhea and colitis in humans and animals (Fabrega and Vila, 2013; Yang et al., 2021). According to reports, *Salmonella* infections are common in both industrialized and developing nations, posing a serious risk to public health and resulting in significant financial losses (Katiyo et al., 2019; Mohan et al., 2019). At present, antibiotics remain one of the most effective treatment strategies for *Salmonella* infections. However, numerous studies have reported that the prolonged use or misuse of antibiotics can lead to environmental pollution, an increase in multi-drug-resistant (MDR) bacteria, as well as gastrointestinal microbiota dysbiosis (Ferri et al., 2017; Paulson et al., 2015; Reyman et al., 2022). In order to tackle *Salmonella* infections, a hunt for novel antimicrobial drugs is now underway.

More research has recently demonstrated the critical role gut microbiota plays in reducing intestinal inflammation (Cristofori et al., 2021) and mending the intestinal barrier (Ohland and Macnaughton, 2010; Wang et al., 2020). The use of probiotics is a popular approach to modulating intestinal microbiota

nowadays. Among all probiotics, *Bacillus* is one of the most popular probiotic species because of its ability to form endospores that survive gastric transit, storage and delivery conditions (Gu et al., 2015). Furthermore, *Bacillus* species can generate extracellular enzymes and antimicrobial metabolites that inhibit enteric pathogens, which lowers the risk of infection and enhances nutrient utilization (Abdhul et al., 2015; Ouattara et al., 2017).

Recent studies have found that *Bacillus velezensis* (*B. velezensis*) has the enormous potential to produce a variety of metabolites with broad-spectrum antibacterial activity (Ye et al., 2018). Meanwhile, previous studies have reported that *B. velezensis* exhibits varying degrees of beneficial effects on plants, livestock, poultry and fish. For instance, the combined use of *B. velezensis* SQR9 mutant and FZB42 improved root colonization and the production of secondary metabolites that are beneficial to cucumber (Shao et al., 2022). *B. velezensis* isolated from yaks was shown to enhance growth performance and ameliorate blood parameters related to inflammation and immunity in mice (Li et al., 2019). The dietary *B. velezensis* supplementation can regulate the innate immune response in the intestine of crucian carp and reduce the degree of intestinal inflammation damage induced by *A. veronii* (Zhang et al., 2019). However, studies on *B. velezensis* in the prevention of *S*. Typhimurium infection are rarely reported; instead, the majority of investigations on *B. velezensis* focused on the biocontrol of fungal infections in plants. In this study, a strain of *B. velezensis* HBXN2020 with broad-

spectrum antibacterial activity against *Salmonella* was selected from a vast number of *Bacillus* strains. Next, we evaluated its safety in mice by supplementing *B. velezensis* HBXN2020 and then explored the protective effects in STm-infected mice. Notably, *B. velezensis* HBXN2020 alleviated colon tissue damage caused by STm infection, as indicated by markers such as STm loads, TNF-α and ZO-1 levels. Moreover, supplementing *B. velezensis* HBXN2020 also increased the abundance of beneficial bacteria, specifically *Lactobacillus* and *Akkermansia*, within the colon microbiota. As a result, this research supports the creation of probiotic-based microbial products as a substitute method of preventing *Salmonella* infections.

Results

Isolation of *Bacillus*

Four strains of *Bacillus* with antibacterial activity were screened from a large amount of presumptive *Bacillus* isolates, based on spot-on-plate tests analysis (Fig. S1), and the four strains clearly displayed the properties of bacteria in the genus *Bacillus* such as colonies were crateriform, Gram-positive, rod shape, and endospore-forming ability. Next, a comparative analysis of the antibacterial spectrum of four strains of *Bacillus* found that one strain exhibited excellent antibacterial activity against common pathogens (Table S1). Therefore, this strain was selected in this study for further research, which was designated as the HBXN2020.

Growth curve and *in vitro* resistance against environmental assaults

The growth of HBXN2020 was assessed in flat-bottomed 100-well microtiter plates by measuring the values of OD_{600} every hour using an automatic growth curve analyzer. After measurement, we found that HBXN2020 entered the logarithmic growth phase after 2 h, and reached a plateau after 10 h of culture (Fig. 1A).

Next, we evaluated the effect of physical, chemical, and biological sterilization conditions such as high temperature, strong acidity, and enzyme preparation on the survival of HBXN2020. The survival rate of HBXN2020 showed a decreasing trend with increasing temperature (Fig. 1B), but this decrease was not obvious. In a strong acid environment (pH 2.0), HBXN2020 maintained a high survival rate (Fig. 1C), suggesting that HBXN2020 spores can survive under extreme conditions. Based on these results, we hypothesized that HBXN2020 spores might also exhibit improved survival in gastrointestinal tract environments. Therefore, we further evaluated the survival rate of HBXN2020 in bile salt (0.3%, v/v), simulated gastric fluid (pepsin 1 mg mL^{-1}, pH 1.2), and simulated intestinal fluid (trypsin 1 mg mL^{-1}, pH 6.8). As shown in Fig. 1D-F, HBXN2020 spores demonstrated significantly improved tolerance to these simulated gastrointestinal tract environments.

Antibiotic susceptibility of HBXN2020 and bacteriostasis effect *in vitro*

In order to assess HBXN2020's drug resistance, 19 antibiotics that are frequently used in clinical settings were chosen in this study. The results indicated that only polymyxin B had a relatively small inhibition zone diameter (less than 15 mm). Ampicillin, meropenem, minocycline, ofloxacin, and trimethoprim had the strongest inhibition on HBXN2020, with an inhibition zone diameter exceeding 30 mm (Fig. 2A). This indicated that HBXN2020 was extremely sensitive to β-lactams, tetracyclines, and quinolone drugs. We next utilized an in vitro antibacterial assay to evaluate the antibacterial activity of HBXN2020. The results showed that HBXN2020 had a similar inhibitory effect on standard and wild strains of *Escherichia coli* (*E. coli*), *Salmonella*, *Staphylococcus aureus* (*S. aureus*), and *Clostridium perfringens* (*C. perfringens*), as well as wild strains of *Streptococcus suis* (*S. suis*), *Pasteurella multocida* (*P. multocida*), and *Actinobacillus pleuropneumoniae* (*A. pleuropneumoniae*). Except for the wild strains of *S. suis* and *A. pleuropneumoniae*, the diameter of the inhibition zone of other strains was above 15 mm (Fig. 2B, S2), while the size of the inhibition zone of *S. suis* and *A. pleuropneumoniae* was also more than 12 mm.

Genomic Characteristics

HBXN2020's complete genome was sequenced using the Illumina Hiseq and PacBio platforms. The results showed that HBXN2020 has a circular chromosome of 3,929,792 bp (Fig. 3A) with a GC content of 46.5%, including

3,744 protein-coding genes (CDS), 86 tRNA genes, and 27 rRNA genes (Table S2). Furthermore, the HBXN2020 genome also contains 13 different clusters of secondary metabolic synthesis genes. such as Fengycin (genomic position:1,865,856) and Difficidin (genomic position:2,270,091) (Table S3).

A phylogenetic tree based on genome-wide data from all 14 *Bacillus* strains demonstrated that the HBXN2020 belongs to the *B. velezensis* species (Fig. 3B). To further understand the classification status of HBXN2020, the online tool JSpeciesWS was used to calculate the average nucleotide identity (ANI) based on the BLAST (ANIb) method. As shown in Fig. S3, HBXN2020 was found to be a member of the *B. velezensis* species due to the high percentage of ANIb (more than 97%).

Safety evaluation of *B. velezensis* HBXN2020

We assessed the *in vivo* effects of *B. velezensis* HBXN2020 in a mouse model in order to ascertain its safety. After gavage with *B. velezensis* HBXN2020 spores for two weeks, we observed no significant difference in the body weight of each group of mice (Fig. 4A). The gene expression levels of TNF-α, IL-1β, IL-6, and IL-10 of colon from all groups of mice exhibited no remarkable changes (Fig. 4B). However, in the colon, mRNA levels of the barrier proteins ZO-1 and occludin were trending towards an increase compared with the control group (Fig. 4C). Additionally, blood routine tests and serum biochemistry tests were performed for mice in the control group

and H-HBXN2020 group on the 14th d after oral administration of *B. velezensis* HBXN2020 spore multiple times. As shown in Fig. 4D and S4, the blood parameters of mice after *B. velezensis* HBXN2020 spores treatment, including red blood cells (RBC), mean corpuscular volume (MCV), mean corpuscular hemoglobin (MCH), hemoglobin (HGB), white blood cells (WBC), platelets (PLT), hematocrit (HCT), and mean corpuscular hemoglobin concentration (MCHC), were consistent with those of healthy mice. The serum biochemical parameters, including alanine aminotransferase (ALT), aspartate aminotransferase (AST), albumin (ALB), total bilirubin (TBIL), serum creatinine (CREA), and blood urea nitrogen (BUN), were also within normal limits (Fig. 4E). The corresponding histological analysis of colon tissue from mice receiving low, medium, and high doses of *B. velezensis* HBXN2020 spores (L-HBXN2020, M-HBXN2020, and H-HBXN2020 groups, respectively) is presented in Fig. 4F. The colon tissue sections of mice in the test groups showed no significant differences compared to the control group. Additionally, there were no observable differences in the major organ tissues (heart, liver, spleen, lung, and kidney) of mice treated with the high dose of *B. velezensis* HBXN2020 spores compared to healthy mice (Fig. S5). The results of this trial show that *B. velezensis* HBXN2020 is safe to use and has no negative side effects in mice.

Oral administration of *B. velezensis* HBXN2020 spores alleviated

infection by *S*. Typhimurium

Testing both solid and liquid co-culture methods to see if *B. velezensis* HBXN2020 might suppress *S.* Typhimurium ATCC14028 (STm), the findings indicated that *B. velezensis* HBXN2020 decreased the development of STm in a dose-dependent manner (Fig. 5A, S6). Next, the therapeutic potential of *B. velezensis* HBXN2020 was evaluated in an STm-infected mouse model. At days 1, 3, and 5 after STm infection, mice in the STm+HBXN2020 group and HBXN2020 group were orally administered *B. velezensis* HBXN2020 spores by gavage, STm+CIP group were given oral ciprofloxacin, while the control group and STm+PBS group were orally treated with sterile PBS (Fig. 5B). Also, the number of excreted STm in feces was counted daily at the designated time points. As shown in Fig. 5C, there was a significant and continuous reduction in the number of STm in feces following treatment with *B. velezensis* HBXN2020 spores or ciprofloxacin, while the number of *B. velezensis* HBXN2020 viable bacteria in feces is also gradually decreasing (Fig. S7A). The number of STm in the mice feces of STm+HBXN2020 group and STm+CIP group exhibited a reduction ranging from 0.12 to 1.18 logs and 0.76 to 1.81 logs respectively, compared with the STm+PBS group, over the period from day 2 to day 7 post-treatment. Moreover, treatment with *B. velezensis* HBXN2020 spore or ciprofloxacin, resulted in a 1.06, 1.69, 1.14 logs and 1.70, 2.15, 1.48 logs reduction in the number of STm in the cecum, colon and ileum, respectively (Fig. 5D-E, S7B). The weight loss ($p < 0.05$) and

Disease Activity Index (DAI) scores ($p < 0.01$) were significantly reduced in mice after *B. velezensis* HBXN2020 spore treatment or ciprofloxacin treatment compared to that in the PBS treatment group (Fig. 5F-G). In addition, we also measured the colon length of the mice and found that the STm+PBS group had a significantly shorter colon length ($p < 0.001$) than the control group and HBXN2020 group. However, compared to the STm+PBS group, the STm+HBXN2020 group ($p < 0.05$) and STm+CIP group exhibited a longer colon (Fig. 5H-I).

Histological analysis further showed that in the control group and HBXN2020 group, the colon epithelial cells and crypt structure were intact with neat villi, while STm+PBS group showed significant histological damage, including erosion or loss of the intestinal epithelium, crypt destruction, and inflammatory cell infiltration in the colonic tissues (Fig. 6A). Compared with the STm+PBS group, *B. velezensis* HBXN2020 and ciprofloxacin protected the mucosal architecture and the loss of intestinal epithelial cells, and reduced inflammatory cell infiltration (Fig. 6A).

To further assess the impact of *B. velezensis* HBXN2020 on intestinal infammatory response, the mRNA levels of inflammatory cytokines in the colonic tissues were measured. As shown in Fig. 6B-D, the mRNA levels of TNF-α ($p < 0.05$), IL-1β ($p < 0.001$), IL-6 ($p <0.001$), and IL-10 ($p <0.001$) in the colon tissue were significantly increased in the STm+PBS group compared to the control group. *B. velezensis* HBXN2020 spore treatment

243 signifcantly decreased the mRNA levels of TNF-α ($p < 0.05$), IL-1β ($p < 0.001$),
244 IL-6 ($p < 0.01$), and increased the IL-10 level, compared with the STm+PBS
245 group. In contrast, ciprofloxacin treatment failed to signifcantly decrease the
246 mRNA levels of IL-6 in the colon of STm-infected mice (Fig. 6D). Similarly,
247 ciprofloxacin treatment drastically dampened the mRNA levels of IL-10 in the
248 colon of STm-infected mice (Fig. 6E).

249 To assess the infuence of *B. velezensis* HBXN2020 on the intestinal barrier
250 integrity, the mRNA levels of tight junction proteins in the colonic tissues were
251 measured. As presented in Fig. 6, compared with control group, the mRNA
252 levels of tight junction protein in the STm+PBS group was significantly
253 reduced, including ZO-1 ($p < 0.05$), occludin ($p < 0.01$), claudin, and Muc2 (p
254 < 0.05) (Fig. 6F-I). Moreover, the levels of tight junction protein transcription
255 were remarkably elevated in the STm+HBXN2020, STm+CIP, and HBXN2020
256 group, including ZO-1 ($p < 0.001$, $p < 0.05$ and $p < 0.05$, respectively),
257 occludin ($p < 0.05$, $p < 0.05$ and $p < 0.01$, respectively), and claudin ($p <$
258 0.001, $p = 0.0857$ and $p < 0.01$, respectively), except for claudin ($p = 0.0857$)
259 in group STm+CIP, compared with that of the STm+PBS group (Fig. 6F-I). In
260 addition, we also detected the transcription level of Muc2 in colon tissue,
261 which mainly exists in and around goblet cells and is an important component
262 of the mucus layer. The transcription levels of Muc2 were dramatically
263 increased in the STm+HBXN2020 group compared with the STm+PBS group
264 (Fig. 6I). Conversely, the mRNA levels of Muc2 were significantly decreased

in the HBXN2020 group and STm+CIP group (Fig. 6I).

Next, we further explore the impact of *B. velezensis* HBXN2020 on the intestinal microbiota composition of STm-treated mice by 16S rRNA gene high throughout sequencing. As shown in Fig. 7, alpha-diversity analysis revealed that both the richness and diversity (calculated in Sobs, Chao, Shannon, and Simpson indexes) were lower in STm+PBS group than control group, HBXN2020 group, STm+HBXN2020 group, and STm+CIP group (Fig. 7A-D). Although an increasing trend of alpha diversity was observed in STm+CIP group, but without statistical difference was achieved as compared with other groups. Principal Components analysis (PCA) based on Bray-Curtis distance showed that a separation in the gut microbiota structure among control and STm+PBS group. When *B. velezensis* HBXN2020 spores were supplemented, the gut microbiota composition of the STm+HBXN2020 group, HBXN2020 group and the control group were closer together (R^2=0.1616, P=0.006, Fig. 7E).

We analyzed the community composition of colonic microbiota at the phylum and genus level, and the results revealed that the composition of the gut microbiota changed markedly after STm-infected mice. At the phylum level, *Bacteroidetes*, *Firmicutes*, *Verrucomicrobiota* and *Proteobacteria* were predominant phyla in the fecal microbiota (Fig. 7F, S8A). At the genus level, infection with STm in the STm+PBS group dramatically reduced the relative abundance of *norank_f_Muribaculaceae*, *Lactobacillus* and *Akkermansia* (Fig.

7G, H-J) and enhanced the abundance of *Enterococcus*, *Salmonella*, *Bacteroides*, *Alloprevotella* and *Escherichia-Shigella* compared to the control group (Fig. 7G, K, S8B). In contrast, the STm+HBXN2020 group and HBXN2020 group significantly improved the relative abundance of *norank_f_Muribaculaceae* ($p = 0.49$, $p < 0.05$,) and *Lactobacillus* ($p < 0.05$, $p < 0.001$) compared with the STm+PBS group (Fig. 7H-I). However, ciprofloxacin treatment significantly decreased the relative abundance of *Lactobacillus* ($p < 0.05$) and *Akkermansia* ($p < 0.05$) compared with the STm+HBXN2020 group (Fig. 7I-J). Differentially abundant fecal bacterial taxa in STm-treated mice in response to *B. velezensis* HBXN2020 and ciprofloxacin were identified by LEfSe analysis (Fig. 7L). Additionally, we found that two bacterial genera including *Enterococcus* and *Streptococcus* were enriched in the STm+PBS group, while the other three taxa were enriched including *Akkermansia*, *Family_XIII_AD3011_group,* and *Corynebacterium* in the STm+HBXN2020 group, *Parabacteroides*, *NK4A214_group*, *Turicibacter*, *unclassified_o__Oscillospirales*, and *norank_f__Eubacterium_coprostanoligenes_group* in the STm+CIP group, and *norank_f_Muribaculaceae*, *Rikenellaceae_RC9_gut_group* and *Dubosiella* in the HBXN2020 group (Fig. 7L).

Prophylactic *B. velezensis* HBXN2020 spores alleviated infection by *S.* Typhimurium

Based on the improved therapeutic efficacy of *B. velezensis* HBXN2020 in the treatment of STm-infected mice, we further explored its potential for disease prevention by evaluating pretreatment. Mice in the PBS+STm group, HBXN2020+STm group, and CIP+STm group were given the same amount of sterile PBS, *B. velezensis* HBXN2020 spores or ciprofloxacin by gavage one week in advance. As shown in Fig. 8, compared with the PBS+STm group, oral administration of *B. velezensis* HBXN2020 spores or ciprofloxacin as a preventive measure remarkably alleviated infection by STm, including weight loss of mice ($p < 0.01$) (Fig. 8B), a significant reduction in DAI ($p < 0.001$) (the comprehensive score of weight loss, stool consistency, and blood in the feces, Fig. 8C), and the prevention of colon length shortening (Fig. 8D-E). Meanwhile, the number of *B. velezensis* HBXN2020 viable bacteria in feces is also gradually decreasing with time prolonging (Fig. S9A). Furthermore, compared with the PBS+STm group, oral administration of *B. velezensis* HBXN2020 spores or ciprofloxacin not only reduced the number of STm in mouse feces (Fig. 8F) but also decreased STm colonization in the ileum, cecum, and colon (Fig. 8G-H, S9B).

Histological analysis further revealed that prophylactic *B. velezensis* HBXN2020 spore suppressed STm induced loss of the intestinal epithelium, inflammatory cell infiltration and colonic mucosa damage (Fig. 9A), while prophylactic ciprofloxacin failed to inhibit the loss of colonic epithelial cells. We next measured the mRNA levels of inflammatory cytokines and tight

junction proteins in colon tissue in the prophylactic animal experiment. As with the treatment test, prophylactic *B. velezensis* HBXN2020 spores largely attenuated the mRNA levels of TNF-α ($p < 0.001$), IL-1β ($p < 0.001$) and IL-6 ($p < 0.001$), and significantly increased levels of IL-10 ($p < 0.05$), in the colon tissue of mice compared with the PBS+STm group (Fig. 9B-E). Similarly, prophylactic ciprofloxacin significantly reduced the mRNA levels of TNF-α ($p < 0.01$) and IL-1β ($p < 0.001$), and drastically elevated levels of IL-10 ($p < 0.001$) in the colon tissue of mice compared with the PBS+STm group (Fig. 9B-C, E). Also, prophylactic *B. velezensis* HBXN2020 spores signifcantly increased the transcription levels of ZO-1 ($p < 0.001$), occludin ($p < 0.001$), claudin ($p < 0.05$), and Muc2 ($p < 0.001$) compared with that of the PBS+STm group (Fig. 9F-I). Notably, the mRNA levels of ZO-1 ($p < 0.001$), occludin ($p < 0.05$), and Muc2 ($p < 0.05$) in the CIP+STm group were significantly lower than those in the HBXN2020+STm group. Overall, these results suggested that prophylactic *B. velezensis* HBXN2020 spores was capable of alleviating STm-induced colonic injury, and inflammation.

Next, we examined the impact of prophylactic *B. velezensis* HBXN2020 on the intestinal microbiota composition of STm-treated mice. Sobs, Chao and Shannon index were signifcantly increased in the HBXN2020, PBS+STm group, HBXN2020+STm group and CIP+STm group compared with the control group (Fig. 10A-C), while the Simpson index (not statistically different) significantly decreased (Fig. 10D). PCA analysis showed significant

separation between control and PBS+STm groups (R^2=0.3186, p=0.014, Fig. 10E). When *B. velezensis* HBXN2020 spores or ciprofloxacin were supplemented, the community clustering was significantly similar to that of the control group rather than the PBS+STm group (Fig. 10E). Meanwhile, the overall fecal bacterial composition of mice at the phylum and genus level in all groups was similar to that of the treatment experiment. The fecal microbiota was dominated by phyla *Firmicutes*, *Bacteroidetes*, *Verrucomicrobiota*, *Patescibacteria*, and *Actinobacteria* in all five groups (Fig. 10F, S10A). At the genus level, PBS+STm group exhibited lower relative abundances of *Lactobacillus* and *Akkermansia* (Fig. 10G, H-I), and higher relative abundances of *Alistipes*, *Bacteroides*, *Escherichia-Shigella*, *Enterococcus*, and *Alloprevotella*, compared with the control (Fig. 10G, J-M, S10B). Moreover, compared with the PBS+STm group, following supplementation with *B. velezensis* HBXN2020 spores or ciprofloxacin, *Lactobacillus* significantly increased, and the gut microbiota was restored to a composition similar to the control group. It was noteworthy that six bacterial genera including *Alistipes*, *Odoribacter*, and *norank_f__Oscillospiraceae* were enriched in PBS+STm group, while other three taxa (e.g., *Lactobacillus* and *Akkermansia*) were enriched in the control group (Fig. 10N). Moreover, we found that *Candidatus_Arthromitus* was enriched in the HBXN2020+STm group, *Dubosiella* was enriched in the CIP+STm group, and *Faecalibaculum*, *Rikenellaceae_RC9_gut_group*, and *unclassified_f__Lactobacillaceae* were

enriched in the HBXN2020 group (Fig. 10N). Above all, these results indicated that prophylactic *B. velezensis* HBXN2020 spores regulated the gut microbiota composition, leading to the potential to attenuate the STm-induced dysbiosis.

Discussion

S. Typhimurium is an important intestinal pathogen that can cause invasive intestinal diseases such as bacterial colitis (Herp et al., 2019; Schultz et al., 2017). Antibiotics are frequently used to treat colitis caused by bacteria; nevertheless, in recent years, their abuse has greatly increased bacterial resistance, leading to serious environmental pollution. A recent study showed that antibiotic-resistance genes in probiotics could be transmitted to the intestinal microbiota, which may threaten human health (Crits-Christoph et al., 2022). It is crucial to consider the source of probiotics. Strong environmental adaptability and disease resistance make black pigs an outstanding household breed in China (Yang et al., 2022). In this study, *B. velezensis* HBXN2020 was isolated from the free-range feces of black piglets in a mountain village in Xianning City (Hubei, China) and exhibited excellent antibacterial activity. Otherwise, *in vitro* tolerance assays showed that *B. velezensis* HBXN2020 spores have good tolerance to high temperature, strong acids, bile salts, as well as simulated gastric and intestinal fluid, which was similar to previous research results (Du et al., 2022). Furthermore,

studies for antibiotic susceptibility revealed that *B. velezensis* HBXN2020 is not resistant to antibiotics.

Probiotics are distinct from food or medications in that they can cause toxins or infections in the body when ingested, and they are living when swallowed (Sanders et al., 2010; Snydman, 2008). Therefore, assessing the biosafety of probiotics is crucial. In this study, the safety of *B. velezensis* HBXN2020 was evaluated by measuring the body weight, intestinal barrier proteins, and inflammatory cytokines of the experimented mice, as well as conducting routine blood and biochemical tests. The results showed that the expression levels of ZO-1 and occludin in the colon of mice increased after treatment with different doses of *B. velezensis* HBXN2020 spores. It has been reported that ZO-1, occludin and claudin are the three most important tight junction proteins in intercellular connections, which play a crucial role in maintaining the intestinal epithelial barrier (Bazzoni et al., 2000; Zihni et al., 2016). Thus, it is possible to improve intestinal barrier function by upregulating ZO-1 and occludin expression levels.

Important aminotransferases in animals, aspartate aminotransferase (AST) and alanine aminotransferase (ALT), are regarded as critical metrics for assessing liver function damage (Gou et al., 2022; Ozer et al., 2008). Under normal circumstances, the levels of ALT and AST are in dynamic balance without notable changes. However, when the liver is damaged or becomes dysfunctional, the levels of aminotransferases (ALT and AST) increase

419 significantly (Tang et al., 2012). Previous studies have shown that CCL4-
420 induced liver injury strongly increases plasma ALT/AST levels (Singhal et al.,
421 2018). Zhang et al. reported that the addition of *Bacillus subtilis* to chicken
422 diets significantly decreased the serum levels of ALT and AST (Zhang et al.,
423 2017). In this present study, the levels of ALT and AST in the probiotic-treated
424 group were slightly lower than those in the control group, indicating that *B.*
425 *velezensis* HBXN2020 had no negative effect on liver health in mice. The *B.*
426 *velezensis* HBXN2020 treatment group's blood indices were also found to be
427 comparable to those of the control group, falling within the normal reference
428 range, according to regular blood testing.

429 Mice were fed with *B. velezensis* HBXN2020 spores orally after being
430 challenged with *S.* Typhimurium ATCC14028 in order to assess the spores'
431 potential to alleviate infection caused by *S*. Typhimurium. Our experimental
432 results demonstrated that oral treatment with *B. velezensis* HBXN2020 spores
433 could alleviate infection by *S*. Typhimurium, as evidenced by decreased
434 weight loss, DAI, and histological damage, which is similar to prior studies
435 (Cao et al., 2019; Wu et al., 2022). Previous research showed that
436 macrophages are the first line of host defense against bacterial infection.
437 They release proinflammatory cytokines, which are critical in initiating
438 adaptive immune responses (Cheng et al., 2014; Dinarello, 2000).
439 Nevertheless, proinflammatory cytokines have immunological properties that
440 can be beneficial for the host to resist the invasion of bacteria and other

microbes in the surrounding environment (Liu et al., 2021). For instance, pretreatment with recombinant murine TNF-α was shown to protect mice against lethal bacterial (*E. coli*) infection (Cross et al., 1989). PJ-34 exerted protective effects on intestinal epithelial cells against invasive *Salmonella* infection by upregulating IL-6 expression through the ERK and NF-κB signal pathways (Huang, 2009).

On the other hand, some research has demonstrated that over-activation of immune cells can result in tissue damage, organ failure, systemic or persistent inflammation, and autoimmune diseases (Karki et al., 2021; Kotas and Medzhitov, 2015). IL-10 is a recognized anti-inflammatory mediator that plays a crucial role in maintaining intestinal microbe-immune homeostasis, regulating the release of inflammatory mediators, and inhibiting proinflammatory responses of innate and adaptive immunity (Maloy and Powrie, 2011; Ouyang et al., 2011; Saraiva et al., 2020). For instance, previous studies have shown that *Clostridium butyrate* can induce the production of IL-10 in the intestine, thereby alleviating experimental colitis in mice (Hayashi et al., 2013). Similar results were observed in our study, where oral administration of *B. velezensis* HBXN2020 spores reduced the expression levels of TNF-α, IL-1β, and IL-6 while increasing the levels of IL-10 in the colon of mice. Additionally, as demonstrated by the decreased histological damage and increased expression levels of intestinal barrier proteins, oral treatment of *B. velezensis* HBXN2020 spores reduced the

functional damage of the intestinal barrier induced by S. Typhimurium infection.

Besides host itself, environmental factors such as diet and gut microbiota have been associated with the development of STm-infected. Gut microbiota constitutes a critical bridge between environmental factors and host health, where the beneficial bacteria such as *Lactobacillus* in the microbiota may exert repair and anti-infammatory function (Li et al., 2022; Liu et al., 2022). Moreover, supplementation of probiotics has been shown to modulate intestinal microbiota and reduce the risk of STm-infected (Buddhasiri et al., 2021; Zhang et al., 2022). This is consistent with our research results between the *B. velezensis* HBXN2020 treatment group and STm-infected mice. Here, we found that oral *B. velezensis* HBXN2020 spores raised the colonic microbiota's alpha diversity and modulated the composition of the intestinal microbiota, namely, enriching the relative abundance of *Lactobacillus* (known for enhancing the epithelial barrier by increasing mucus secretion and upregulating the expression of tight junction proteins such as claudin-1, occludin, and ZO-1) (Kaur et al., 2021) and *Akkermansia* (known for modulating intestinal immune response by producing short chain fatty acids and reducing the secretion of proinflammatory cytokines) (Cani et al., 2022), reducing the relative abundance of *Enterococcus*, *Salmonella* and *Bacteroides* (harmful to intestinal homeostasis) (Wang et al., 2023). Notably, we also found that the relative abundance of *Lactobacillus* and *Akkermansia*

in the ciprofloxacin treatment group was significantly lower than that in the *B. velezensis* HBXN2020 spores treatment group, indicating that excessive use of antibiotics may interfere with the recovery of beneficial bacteria in the gut. Collectively, infection with *S*. Typhimurium disrupts gut microbiota and the gut barrier, leading to intestinal inflammation, while oral *B. velezensis* HBXN2020 spores protects the colon and reduce infection by increasing the abundance of beneficial bacteria and and barrier integrity and decreasing inflammation.

We further assessed pretreatment in order to learn more about the potential of *B. velezensis* HBXN2020 spores for disease prevention, given the increased efficacy of treating infection caused by *S*. Typhimurium. Similarly to the therapeutic effect of oral *B. velezensis* HBXN2020, prophylactic *B. velezensis* HBXN2020 spores effectively alleviated the symptoms of STm-infected mice, namely, reduced the mRNA levels of proinflammatory cytokines and increased the anti-inflammatory cytokine level in the colon of STm-infected mice. Prophylactic *B. velezensis* HBXN2020 spores also increased the mRNA levels of gut barrier proteins in the colon of STm-infected mice. Furthermore, the microbiota composition was also dramatically modulated by prophylactic *B. velezensis* HBXN2020 spores in both healthy mice and STm-infected mice. Also, the community richness revealed by the alpha diversity index were not significantly impacted in STm-infected mice by prophylactic *B. velezensis* HBXN2020 spores. Interestingly, we found that prophylactic *B. velezensis* HBXN2020 spores signifcantly increased the community diversity

in healthy mice, suggesting the potentially benefcial efects of *B. velezensis* HBXN2020 in gut microenvironment for animals in the future. Moreover, prophylactic *B. velezensis* HBXN2020 spores significantly boosted SCFA-producing bacteria including *Lactobacillus* and *Akkermansia*, which was consistent with the effects of therapeutic oral *B. velezensis* HBXN2020 spores. Meanwhile, harmful bacteria such as *Alistipes*, *Bacteroides*, *Escherichia-Shigella*, and *Enterococcus* were significantly enriched in STm-infected mice, reminding us that increased harmful bacteria might play a major role in promoting the development of STm-infected. In summary, our results demonstrated that *B. velezensis* HBXN2020-mediated microbial communities, especially *Lactobacillus* and *Akkermansia* might play a crucial role in alleviating the development of STm-infected.

Conclusion

In conclusion, *S*. Typhimurium ATCC14028 infection can result in gut barrier disruption and intestinal inflammation and intestinal microbiota dysbiosis. Supplementing *B. velezensis* HBXN2020 spores can improve intestinal microbiota stability and gut barrier integrity and reduce inflammation to help prevent or treat infection by *S*. Typhimurium. Thus, our results indicate that supplementing *B. elezensis* HBXN2020 may represent a novel option for preventing *Salmonella* infections.

Experimental procedures

Sample collection and strain isolation

Fresh fecal samples were collected from the farms of various locations in southern China including Hubei, Anhui, Hunan, Jiangxi, Guizhou, and Guangxi. All samples were placed in sterile plastic bags, sealed and placed on ice, and immediately transported to the laboratory. *Bacillus* was isolated following a previously described method with slight modification (Unban et al., 2020). The obtained strains were kept in Luria-Bertani (LB) media containing 25% (v/v) glycerol and stored at −80°C, and prepared in LB medium or LB-Agar medium before use.

Antibacterial activity of *Bacillus*

The antibacterial activity of *Bacillus* isolates was evaluated by using the spot-on-plate method on LB agar plates supplemented with indicator bacteria (*Salmonella*, *E. coli*, *S. aureus*). Briefly, an overnight culture of indicator bacteria was dipped by sterile cotton swabs and spread on LB agar plates. *Bacillus* solution was spotted onto the double-layer agar plates and incubated at 37°C for 12 h to measure the inhibition zone. A transparent zone of at least 1 mm around the spot was considered positive.

The antibacterial spectrum of *Bacillus* isolates was compared through the agar diffusion test, based on the results of the spot-on-plate test. In brief, an overnight culture of indicator strains was mixed with 10 mL of TSB soft agar (TSB broth containing 0.7% [wt/vol] agar) and poured into a sterile plate

covered with LB agar and Oxford cups, 8 mm diameter wells were prepared in the TSB agar after removing the cups. The wells were filled with 100 μL of *Bacillus* solution. The plates were incubated at 37°C for 14 h, and the inhibition zone was measured.

The indicator strains used in this study are listed in Table S4, and all the primers used in Table S5. *Clostridium perfringens* were cultured in a fluid thioglycollate medium (FTG) (Hopebio, Qingdao, China) at 45°C. *Streptococcus suis* and *Pasteurella multocida* were cultured in TSB medium supplemented with 5% (v/v) sheep serum (Solarbio, Beijing, China) at 37°C, and *Actinobacillus pleuropneumoniae* were cultured in TSB supplemented with 5% (v/v) sheep serum and 5mM nicotinamide adenine dinucleotide (NAD) at 37°C, while the other bacterial strains were cultured in Luria Bertani (LB) medium (Solarbio, Beijing, China) at 37°C. In addition, the Difco sporulation medium (DSM) was used for inducing the sporulation of *Bacillus* via the nutrient depletion method (Tang et al., 2017).

Growth curves of HBXN2020

The growth curve of HBXN2020 was recorded in flat-bottomed 100-well microtiter plates via detecting optical density at 600 nm (OD_{600}) at 1 h intervals using the automatic growth curve analyzer (Bioscreen, Helsinki, Finland).

In vitro resistance assay of HBXN2020

HBXN2020 spores (100 μL) or vegetative cells (100 μL) were separately resuspended in 900 μL of LB medium supplemented with different pH values (2, 3, 4, 5 or 6), bile salts (0.85% NaCl, 0.3%), simulated gastric fluid (SGF, HCl, pH 1.2) containing 10 g L^{-1} of pepsin in 0.85% NaCl solution, or simulated intestinal fluid (SIF, NaOH, pH 6.8) containing 10 g L^{-1} of trypsin in 0.05 M KH2PO4 solution, and incubated at 37 °C. A normal LB medium (pH 7.0) was used as the control. At predetermined time points, 100 μL was taken from each sample, serially diluted 10-fold with sterile PBS (pH 7.2), and then spread onto LB agar plates. The plates were incubated overnight in a constant temperature incubator at 37°C, and the bacterial colonies were counted. The survival rate was calculated using the following formula: Survival rate = (number of bacteria in the treatment group/number of bacteria in the control group) × 100%.

One milliliter of HBXN2020 spores or vegetative cells were separately placed in water baths at different temperatures (37°C, 45°C, 55°C, 65°C, 75°C, 85°C or 95°C) for 20 min, with a 37°C water bath used as the control. The survival rate was calculated as described above.

Antibiotic susceptibility assays

Antimicrobial susceptibility testing was performed using the Kirby-Bauer (KB) disk diffusion method in accordance with the Clinical Laboratory

Standards Institute (CLSI) guidelines (CLSI., 2018.). The antimicrobial agents tested were: Ampicillin, Meropenem, Piperacillin, Gentamycin, Tetracycline, Doxycycline, Minocycline, Erythromycin, Enrofloxacin, Ofloxacin, Sulfamethoxazole, Trimethoprim-sulfamethoxazole, Polymyxin B, Teicoplanin, Trimethoprim, Florfenicol, Spectinomycin, Nitrofurantoin, and Rifampicin. The diameter of the inhibition zone was measured using a vernier caliper.

Antimicrobial Assays

The *in vitro* antagonistic activity of HBXN2020-CFS was tested using the agar well-diffusion method against 18 indicator strains (pathogens), which included 7 standard strains (*E. coli* ATCC 25922, *E. coli* ATCC 35150, *S.* Typhimurium ATCC 14028 (STm), *S.* Typhimurium SL1344, *S. aureus* ATCC 29213, *S. aureus* ATCC 43300, and *C. perfringens* CVCC 2030) and 11 clinical isolates (*E. coli* EC024, *S.* Enteritidis SE006, *S. aureus* S21, *C. perfringens* CP023, *C. perfringens* CP002, *S. suis* SC19, *S. suis* SS006, *P. multocida* PM002, *P. multocida* PM008, *A. pleuropneumoniae* APP015, and *A. pleuropneumoniae* APP017). All plates were cultured at 37°C for 16 h before observing the inhibition zone, and the diameter of the inhibition zone was measured using a vernier caliper. The presence of a clear zone indicated antagonistic activity.

***In vitro* bacterial competition.**

To investigate whether HBXN2020 directly inhibited the growth of STm, we performed spot-on lawn and agar-well diffusion assays, as well as co-culture assays in liquid culture medium. In the spot-on lawn antimicrobial assays, we prepared double layers of agar by first pouring LB agar into the plate as the bottom layer. The top layer consisted of 10 mL TSB broth containing 0.7% agar with STm overnight culture. Then, 10 μL of HBXN2020 overnight culture and cell-free supernatant (CFS) were respectively spotted onto TSB agar and incubated at 37°C for 12 h to measure the inhibition zone. A transparent zone of at least 1 mm around the spot was considered positive.

The antagonistic effect of HBXN2020-CFS against STm was determined using the agar-well diffusion assays. To collect HBXN2020-CFS, the culture was centrifuged at 9,000g for 15 min at 4°C, and the supernatant was filtered through a 0.22 μm membrane filter (Millipore, USA). The STm lawn medium was prepared by mixing 10 mL of TSB broth containing 0.7% agar with STm overnight culture and then poured into a sterile plate covered with LB agar and Oxford cups, 8 mm diameter wells were prepared in the TSB agar after removing the cups. The wells were filled with 100 μL of HBXN2020-CFS, LB medium or ampicillin (100 μg mL^{-1}). The plates were incubated at 37°C for 14 h, and the inhibition zone was measured.

The co-culture assay was conducted by incubating HBXN2020 and *S.* Typhimurium ATCC14028 (carry pET28a (+), kanamycin resistance) (Cao et al., 2019) separately overnight at 37°C and diluting them to 10^4 CFU/mL.

Then, the two strains were mixed at different ratios (1:1, 1:10, 1:50 or 1:100) and co-cultured at 37°C with shaking (180 rpm). At predetermined time points, serial 10-fold dilutions were prepared for all samples and spread onto selective (kanamycin 50 μg mL^{-1}) LB agar plates and cultured at 37°C for 12 h before bacterial counting. Viable colony counts ranged from 30 to 300 per plate.

Genome sequencing, annotation and analysis

The complete genome of strain was sequenced using the Illumina HiSeq PE and PacBio RSII (SMRT) platforms (Shanghai Majorbio Bio-pharm Technology Co., Ltd.). Briefly, the short reads from the Illumina HiSeq PE were assembled into contigs using SPAdenovo (http://soap.genomics.org.cn/). The long reads from the PacBio RSII and the Illumina contigs were then aligned using the miniasm and Racon tools in Unicycler (version 0.4.8, https://github.com/rrwick/Unicycler) to generate long-read sequences. During the assembly process, sequence correction was performed using Pilon (version 1.22, https://github.com/broadinstitute/pilon/wiki/Standard-Output). Lastly, a complete genome with seamless chromosomes was obtained.

The coding sequences (CDs) of the strain genome were predicted using Glimmer (version 3.02, http://ccb.jhu.edu/software/glimmer/index.shtml). The tRNA and rRNA genes were predicted using TRNAscan-SE (version 2.0, http://trna.ucsc.edu/software/) and Barrnap (version 0.8,

https://github.com/tseemann/barrnap), respectively. The functional annotation of all CDSs was performed using various databases, including Swiss-Prot Database (https://web.expasy.org/docs/swiss-prot_guideline.html), Pfam Database (http://pfam.xfam.org/), EggNOG Database (http://eggnog.embl.de/), GO Database (http://www.geneontology.org/), and KEGG Database (http://www.genome.jp/kegg/). The circular map of the strain genome was generated using CGView (version 2, http://wishart.biology.ualberta.ca/cgview/) (Stothard and Wishart, 2005).

Comparative genomic analysis

To elucidate the phylogenetic relationships of the strain from a whole-genome perspective, a phylogenetic tree based on the whole genome was constructed using the Type (Strain) Genome Server (TYGS) online (https://ggdc.dsmz.de/) (Meier-Kolthoff et al., 2022). The average nucleotide identity (ANI) values of the strain genome to the reference strain genome were then calculated using the JSpeciesWS online service (Richter et al., 2016), and a heatmap was generated using TBtools (version 1.113) (Chen et al., 2020).

***In vivo* safety evaluation of *B. velezensis* HBXN2020**

Female specific-pathogen-free (SPF) C57BL/6 mice aged 6 to 8 weeks were purchased from the Animal Experimental Center of Huazhong

Agricultural University. All mice experiments were conducted in the standard SPF facility of Huazhong Agricultural University, with 12 h of light and 12 h of darkness at a temperature of 25°C and ad libitum access to food and water. The use of animals in this experiment was approved by the Animal Care and Ethics Committee of Huazhong Agricultural University (Ethics Approval Number: HZAUMO-2023-0089).

Safety assay of *B. velezensis* HBXN2020 referred to the method described by Zhou et al. (Zhou et al., 2022) with slight modifications. After a 7-day acclimation period (free access to water and food), mice were randomly divided into four treatment groups (n = 5): low-dose *B. velezensis* HBXN2020 spores group (L-HBXN2020 group, 10^7 CFU/mouse), medium-dose *B. velezensis* HBXN2020 spores group (M-HBXN2020 group, 10^8 CFU/mouse), high-dose *B. velezensis* HBXN2020 spores group (H-HBXN2020 group, 10^9 CFU/mouse), and a control group. During the experimental period (15 days), mice were weighed and orally gavaged with their respective treatments once every two days. On day 15, all mice were euthanized, and blood, heart, liver, spleen, lung, kidney, ileum, cecum, and colon were collected. Blood samples were used for routine blood and biochemistry tests. Major organ tissues (heart, liver, spleen, lung, and kidney) and a 5-mm distal segment of the colon were used for histopathology. The remaining colonic tissues were rapidly frozen in liquid nitrogen and stored at −80°C for cytokine and tight junction protein expression analysis.

705

706 ***Salmonella* Typhimurium-infected mouse model**

707 After 7 days of acclimation (free access to water and food), mice were
708 randomly divided into five treatment groups (n = 6): control group, HBXN2020
709 group, STm+PBS group, STm+HBXN2020 group and STm+CIP group. The *S.*
710 Typhimurium-infected model was performed as previously described (Stecher
711 et al., 2005), with slight modifications. On the first day of the experiment, all
712 mice in the STm+PBS group, STm+HBXN2020 group and STm+CIP group
713 were orally inoculated with 200 μL (5×10^7 CFU/mouse) of STm. On days 1, 3
714 and 5 following STm infection, each mouse in the HBXN2020 group,
715 STm+HBXN2020 group and STm+CIP group received 200 μL (1×10^8
716 CFU/mouse) of *B. velezensis* HBXN2020 spores or ciprofloxacin (1 mg/mL)
717 via gavage administration, respectively. In contrast, the control group and
718 STm+PBS group received 200 μL of sterile PBS by oral gavage. Fecal
719 samples were collected daily following STm infection and resuspended in
720 sterile PBS. The number of STm in mice feces from both the STm+PBS,
721 STm+HBXN2020 and STm+CIP groups was then determined by spreading a
722 serial 10-fold dilution on selective LB agar plates containing 50 μg mL^{-1}
723 kanamycin. Throughout the entire experiment, the body weight, stool
724 consistency and fecal occult blood of all mice were monitored daily. As shown
725 in Table S6, disease activity index (DAI) was calculated by the sum of the
726 scores from three parameters (Praveschotinunt et al., 2019). On day 7 after

STm infection, all mice were euthanized, their ileum, cecum and colon were collected. The length of colon was measured, and a 5-mm distal segment of the colon was fixed in 4% paraformaldehyde for further histopathology. The remaining colon was then rapidly frozen in liquid nitrogen and stored at −80°C for cytokine and tight junction protein expression analysis. Then, the number of STm in the ileum, cecum, and colon was determined by spreading serial 10-fold dilutions on selective LB agar plates.

To investigate the prophylactic efficacy of *B. velezensis* HBXN2020 in ameliorating STm-infected, another independent experiment was conducted using six-week-old female C57BL/6 mice (SPF). After a seven-day acclimation period, mice were randomly assigned to five groups (n = 6): control group, HBXN2020 group, PBS+STm group, HBXN2020+STm group and CIP+STm group. On days 1, 3, 5 and 7, each mouse in the HBXN2020 group, HBXN2020+STm group and CIP+STm group received 200 μL (1×10^8 CFU/mouse) of *B. velezensis* HBXN2020 spores or ciprofloxacin (1 mg/mL) via gavage administration. Meanwhile, mice in the control group and PBS+STm group received 200 μL of sterile PBS by oral gavage. On day 7, all mice in the PBS+STm group, HBXN2020+STm group and CIP+STm group were orally inoculated with 200 μL (5×10^7 CFU/mouse) of STm. Fecal samples were collected daily following STm infection from both groups and resuspended in sterile PBS. The number of STm in the feces of mice was then determined by spreading serial 10-fold dilutions on selective LB agar

plates (50 μg mL^{-1} kanamycin). Throughout the entire experiment, the body weight and DAI scores of all mice were monitored daily. On day 12, all mice were euthanized, and the ileum, cecum, and colon were collected. The colon length was measured, and a 5-mm distal segment of the colon was fixed in 4% formalin for sectioning and staining. The remaining colon was stored at −80°C for future analysis. Lastly, the number of STm in the ileum, cecum, and colon was determined using a selective LB agar plate.

Determination of cytokines and tight junction protein expression in colon tissue

Total RNA was extracted from colon tissues using TRIpure reagent (Aidlab, China), and cDNA was obtained using HiScript® III RT SuperMix for qPCR (+gDNA wiper) (Vazyme, China). RT-qPCR for each gene was performed in triplicate using qPCR SYBR Green Master Mix (Yeasen Biotechnology, Shanghai, China). The relative expression level of cytokine and tight junction protein genes was calculated using the $2^{-\Delta\Delta Ct}$ method with β-actin and GAPDH as reference genes. The primer sequences used in the RT-qPCR test are listed in Table S5.

Histopathology analysis

Colon tissue samples (0.5 cm) were fixed in 4% paraformaldehyde for 24 h, and the fixed tissues were then embedded in paraffin and sectioned. The

sections were stained with hematoxylin and eosin (H&E) and observed and imaged using an optical microscope (Olympus Optical, Tokyo, Japan). The histopathological score included the degree of inflammatory infiltration, changes in crypt structures, and the presence or absence of ulceration and edema. The scoring criteria were determined as previously described (Wu et al., 2022).

16S rRNA gene sequencing and analysis

According to the manufacturer's instructions, colon microbial community genomes were extracted using E.Z-N.A ® Stool DNA Kit (Omega; D4015-01), and quality was detected by 1% agarose gel electrophoresis. The 16S rRNA V3-V4 variable region was amplified by PCR using universal primers 338F (5 '- ACTCCTACGGGGGGCAG-3') and 806R (5 '- GACTACHVGGGTWTCTAAT-3'). The PCR products were examined by electrophoresis on 2% agarose gels and then purified with the AxyPrep DNA gel extraction kit (Axygen Biosciences, USA). A sequencing library was constructed using the NEXTFLEX® Rapid DNA-Seq Kit, and sequencing was performed using the Illumina MiSeq platform. Raw reads were quality evaluated and filtered by fastp (version 0.20.0) and merged using FLASH (version 1.2.7). The optimized sequences were clustered into operational taxonomic units (OTUs) based on 97% sequence similarity using UPARSE (version 7.1). The representative sequences of each OTU was classified by

RDP classifier (version 2.2; confidence threshold value, 0.7). Alpha diversity was assessed using the ACE, chao, Shannon, and Simpson indices. The β-diversity analysis was performed using Bray-Curtis distances and visualized through principal component analysis (PCA). Linear discriminant analysis (LDA) effect size (LefSe) was used to identify differential microbiota between groups.

Statistical Analysis

Statistical analysis was performed using GraphPad Prism 8.3.0 (GraphPad Software, San Diego, CA, USA) and Excel (Microsoft, Redmond, USA). Data are presented as mean ± standard error of the mean (SEM). Differences between two groups were evaluated using two-tailed unpaired Student's t-test, and all other comparisons were conducted using one-way analysis of variance (ANOVA) with Tukey's multiple comparisons test. For all analyses, significance differences are denoted as: *, $p < 0.05$, **, $p < 0.01$, and ***, $p < 0.001$.

Data availability

The datasets supporting the conclusions of this article were deposited in the NCBI Sequence Read Archive database under the accession numbers: CP119399.1 (whole genome sequencing raw data) and PRJNA1150571 (microbiota raw sequencing data).

Conflict of interest: We declare no conflict of interest.

ACKNOWLEDGMENTS

This work was supported by grants from the National Program on Key Research Project of China (2021YFD1800300, 2022YFD1800800), “Yingzi Tech & Huazhong Agricultural University Intelligent Research Institute of Food Health” (No. IRIFH202209; IRIFH202301), and the Fundamental Research Funds for the Central Universities (2662016PY004).

Author contributions

Linkang Wang: Conceptualization, Methodology, Data curation, Formal analysis, Writing - original draft. **Haiyan Wang, Xinxin Li, Mengyuan Zhu**: Methodology, Data curation, Planned and performed the experiments. **Dongyang Gao, Dayue Hu, Zhixuan Xiong**: Methodology, Writing - Reviewing and Editing. **Xiangmin Li**: Supervision, Writing-reviewing and editing. **Ping Qian**: Conceptualization, Funding acquisition, Project administration, Supervision, Writing-Reviewing and Editing. All authors read and approved the submitted version of the paper.

Funding information

This work was supported by grants from the National Program on Key

Research Project of China (2021YFD1800300, 2022YFD1800800), “Yingzi Tech & Huazhong Agricultural University Intelligent Research Institute of Food Health” (No. IRIFH202209; IRIFH202301), and the Fundamental Research Funds for the Central Universities (2662016PY004).

Reference

Abdhul, K., Ganesh, M., Shanmughapriya, S., Vanithamani, S., Kanagavel, M., Anbarasu, K., and Natarajaseenivasan, K. (2015). Bacteriocinogenic potential of a probiotic strain Bacillus coagulans [BDU3] from Ngari. Int J Biol Macromol *79*, 800-806.

Bazzoni, G., Martinez-Estrada, O.M., Orsenigo, F., Cordenonsi, M., Citi, S., and Dejana, E. (2000). Interaction of junctional adhesion molecule with the tight junction components ZO-1, cingulin, and occludin. J Biol Chem *275*, 20520-20526.

Buddhasiri, S., Sukjoi, C., Kaewsakhorn, T., Nambunmee, K., Nakphaichit, M., Nitisinprasert, S., and Thiennimitr, P. (2021). Anti-inflammatory Effect of Probiotic Limosilactobacillus reuteri KUB-AC5 Against Salmonella Infection in a Mouse Colitis Model. Front Microbiol *12*, 716761.

Cani, P.D., Depommier, C., Derrien, M., Everard, A., and de Vos, W.M. (2022). Akkermansia muciniphila: paradigm for next-generation beneficial microorganisms. Nat Rev Gastroenterol Hepatol *19*, 625-637.

Cao, Z., Wang, X., Pang, Y., Cheng, S., and Liu, J. (2019). Biointerfacial self-assembly generates lipid membrane coated bacteria for enhanced oral delivery and treatment. Nat Commun *10*, 5783.

Chen, C., Chen, H., Zhang, Y., Thomas, H.R., Frank, M.H., He, Y., and Xia, R. (2020). TBtools: An Integrative Toolkit Developed for Interactive Analyses of Big Biological Data. Mol Plant *13*, 1194-1202.

Cheng, A., Yan, H., Han, C., Wang, W., Tian, Y., and Chen, X. (2014). Polyphenols from blueberries modulate inflammation cytokines in LPS-induced RAW264.7 macrophages. Int J Biol Macromol *69*, 382-387.

CLSI. (2018.). Performance standards for antimicrobial disk susceptibility tests, M02, 13th ed. Clinical and Laboratory Standards Institute, Wayne, PA.

Cristofori, F., Dargenio, V.N., Dargenio, C., Miniello, V.L., Barone, M., and Francavilla, R. (2021). Anti-Inflammatory and Immunomodulatory Effects of Probiotics in Gut Inflammation: A Door to the Body. Front Immunol *12*, 578386.

Crits-Christoph, A., Hallowell, H.A., Koutouvalis, K., and Suez, J. (2022). Good microbes, bad genes? The dissemination of antimicrobial resistance in the human microbiome. Gut Microbes *14*, 2055944.

Cross, A.S., Sadoff, J.C., Kelly, N., Bernton, E., and Gemski, P. (1989). Pretreatment with recombinant murine tumor necrosis factor alpha/cachectin and murine interleukin 1 alpha protects mice from lethal bacterial infection. J Exp Med *169*, 2021-2027.

Dinarello, C.A. (2000). Proinflammatory cytokines. Chest *118*, 503-508.

Du, H., Yao, W., Kulyar, M.F., Ding, Y., Zhu, H., Pan, H., Li, K., Bhutta, Z.A., Liu, S., and Li, J. (2022). Effects of Bacillus amyloliquefaciens TL106 Isolated from Tibetan Pigs on Probiotic Potential and Intestinal Microbes in Weaned Piglets. Microbiol Spectr *10*, e0120521.

875 Fabrega, A., and Vila, J. (2013). Salmonella enterica serovar Typhimurium skills to succeed in the host:
876 virulence and regulation. Clin Microbiol Rev *26*, 308-341.
877 Ferri, M., Ranucci, E., Romagnoli, P., and Giaccone, V. (2017). Antimicrobial resistance: A global
878 emerging threat to public health systems. Crit Rev Food Sci Nutr *57*, 2857-2876.
879 Gou, S., Chen, N., Wu, X., Zu, M., Yi, S., Ying, B., Dai, F., Ke, B., and Xiao, B. (2022). Multi-responsive
880 nanotheranostics with enhanced tumor penetration and oxygen self-producing capacities for
881 multimodal synergistic cancer therapy. Acta Pharm Sin B *12*, 406-423.
882 Gu, S.B., Zhao, L.N., Wu, Y., Li, S.C., Sun, J.R., Huang, J.F., and Li, D.D. (2015). Potential probiotic
883 attributes of a new strain of Bacillus coagulans CGMCC 9951 isolated from healthy piglet feces. World
884 J Microbiol Biotechnol *31*, 851-863.
885 Hayashi, A., Sato, T., Kamada, N., Mikami, Y., Matsuoka, K., Hisamatsu, T., Hibi, T., Roers, A., Yagita, H.,
886 Ohteki, T., *et al.* (2013). A single strain of Clostridium butyricum induces intestinal IL-10-producing
887 macrophages to suppress acute experimental colitis in mice. Cell Host Microbe *13*, 711-722.
888 Herp, S., Brugiroux, S., Garzetti, D., Ring, D., Jochum, L.M., Beutler, M., Eberl, C., Hussain, S., Walter, S.,
889 Gerlach, R.G., *et al.* (2019). Mucispirillum schaedleri Antagonizes Salmonella Virulence to Protect Mice
890 against Colitis. Cell Host Microbe *25*, 681-694 e688.
891 Huang, F.C. (2009). Upregulation of Salmonella-induced IL-6 production in Caco-2 cells by PJ-34, PARP-
892 1 inhibitor: involvement of PI3K, p38 MAPK, ERK, JNK, and NF-kappaB. Mediators Inflamm *2009,*
893 103890.
894 Karki, R., Sharma, B.R., Tuladhar, S., Williams, E.P., Zalduondo, L., Samir, P., Zheng, M., Sundaram, B.,
895 Banoth, B., Malireddi, R.K.S., *et al.* (2021). Synergism of TNF-alpha and IFN-gamma Triggers
896 Inflammatory Cell Death, Tissue Damage, and Mortality in SARS-CoV-2 Infection and Cytokine Shock
897 Syndromes. Cell *184*, 149-168 e117.
898 Katiyo, S., Muller-Pebody, B., Minaji, M., Powell, D., Johnson, A.P., De Pinna, E., Day, M., Harris, R., and
899 Godbole, G. (2019). Epidemiology and Outcomes of Nontyphoidal Salmonella Bacteremias from
900 England, 2004 to 2015. J Clin Microbiol *57*.
901 Kaur, H., Gupta, T., Kapila, S., and Kapila, R. (2021). Protective effects of potential probiotic
902 Lactobacillus rhamnosus (MTCC-5897) fermented whey on reinforcement of intestinal epithelial
903 barrier function in a colitis-induced murine model. Food Funct *12*, 6102-6116.
904 Kotas, M.E., and Medzhitov, R. (2015). Homeostasis, inflammation, and disease susceptibility. Cell *160*,
905 816-827.
906 Li, A., Wang, Y., Li, Z., Qamar, H., Mehmood, K., Zhang, L., Liu, J., Zhang, H., and Li, J. (2019). Probiotics
907 isolated from yaks improves the growth performance, antioxidant activity, and cytokines related to
908 immunity and inflammation in mice. Microb Cell Fact *18*, 112.
909 Li, H., Cheng, S., Huo, J., Dong, K., Ding, Y., Man, C., Zhang, Y., and Jiang, Y. (2022). Lactobacillus
910 plantarum J26 Alleviating Alcohol-Induced Liver Inflammation by Maintaining the Intestinal Barrier
911 and Regulating MAPK Signaling Pathways. Nutrients *15*.
912 Liu, C., Chu, D., Kalantar-Zadeh, K., George, J., Young, H.A., and Liu, G. (2021). Cytokines: From Clinical
913 Significance to Quantification. Adv Sci (Weinh) *8*, e2004433.
914 Liu, Z., Zhao, J., Sun, R., Wang, M., Wang, K., Li, Y., Shang, H., Hou, J., and Jiang, Z. (2022). Lactobacillus
915 plantarum 23-1 improves intestinal inflammation and barrier function through the TLR4/NF-κB
916 signaling pathway in obese mice. Food Funct *13*, 5971-5986.
917 Maloy, K.J., and Powrie, F. (2011). Intestinal homeostasis and its breakdown in inflammatory bowel
918 disease. Nature *474*, 298-306.

919 Meier-Kolthoff, J.P., Carbasse, J.S., Peinado-Olarte, R.L., and Goker, M. (2022). TYGS and LPSN: a
920 database tandem for fast and reliable genome-based classification and nomenclature of prokaryotes.
921 Nucleic Acids Res *50*, D801-D807.
922 Mohan, A., Munusamy, C., Tan, Y.C., Muthuvelu, S., Hashim, R., Chien, S.L., Wong, M.K., Khairuddin,
923 N.A., Podin, Y., Lau, P.S., *et al.* (2019). Invasive Salmonella infections among children in Bintulu,
924 Sarawak, Malaysian Borneo: a 6-year retrospective review. BMC Infect Dis *19*, 330.
925 Ohland, C.L., and Macnaughton, W.K. (2010). Probiotic bacteria and intestinal epithelial barrier
926 function. Am J Physiol Gastrointest Liver Physiol *298*, G807-819.
927 Ouattara, H.G., Reverchon, S., Niamke, S.L., and Nasser, W. (2017). Regulation of the synthesis of pulp
928 degrading enzymes in Bacillus isolated from cocoa fermentation. Food Microbiol *63*, 255-262.
929 Ouyang, W., Rutz, S., Crellin, N.K., Valdez, P.A., and Hymowitz, S.G. (2011). Regulation and functions of
930 the IL-10 family of cytokines in inflammation and disease. Annu Rev Immunol *29*, 71-109.
931 Ozer, J., Ratner, M., Shaw, M., Bailey, W., and Schomaker, S. (2008). The current state of serum
932 biomarkers of hepatotoxicity. Toxicology *245*, 194-205.
933 Paulson, J.A., Zaoutis, T.E., Council on Environmental, H., and Committee on Infectious, D. (2015).
934 Nontherapeutic Use of Antimicrobial Agents in Animal Agriculture: Implications for Pediatrics.
935 Pediatrics *136*, e1670-1677.
936 Praveschotinunt, P., Duraj-Thatte, A.M., Gelfat, I., Bahl, F., Chou, D.B., and Joshi, N.S. (2019).
937 Engineered E. coli Nissle 1917 for the delivery of matrix-tethered therapeutic domains to the gut. Nat
938 Commun *10*, 5580.
939 Reyman, M., van Houten, M.A., Watson, R.L., Chu, M., Arp, K., de Waal, W.J., Schiering, I., Plotz, F.B.,
940 Willems, R.J.L., van Schaik, W., *et al.* (2022). Effects of early-life antibiotics on the developing infant gut
941 microbiome and resistome: a randomized trial. Nat Commun *13*, 893.
942 Richter, M., Rossello-Mora, R., Oliver Glockner, F., and Peplies, J. (2016). JSpeciesWS: a web server for
943 prokaryotic species circumscription based on pairwise genome comparison. Bioinformatics *32*, 929-
944 931.
945 Sanders, M.E., Akkermans, L.M., Haller, D., Hammerman, C., Heimbach, J., Hormannsperger, G., Huys,
946 G., Levy, D.D., Lutgendorff, F., Mack, D., *et al.* (2010). Safety assessment of probiotics for human use.
947 Gut Microbes *1*, 164-185.
948 Saraiva, M., Vieira, P., and O'Garra, A. (2020). Biology and therapeutic potential of interleukin-10. J Exp
949 Med *217*.
950 Schultz, B.M., Paduro, C.A., Salazar, G.A., Salazar-Echegarai, F.J., Sebastian, V.P., Riedel, C.A., Kalergis,
951 A.M., Alvarez-Lobos, M., and Bueno, S.M. (2017). A Potential Role of Salmonella Infection in the Onset
952 of Inflammatory Bowel Diseases. Front Immunol *8*, 191.
953 Shao, J., Liu, Y., Xie, J., Stefanic, P., Lv, Y., Fan, B., Mandic-Mulec, I., Zhang, R., Shen, Q., and Xu, Z.
954 (2022). Annulment of Bacterial Antagonism Improves Plant Beneficial Activity of a Bacillus velezensis
955 Consortium. Appl Environ Microbiol *88*, e0024022.
956 Singhal, M., Liu, X., Inverso, D., Jiang, K., Dai, J., He, H., Bartels, S., Li, W., Abdul Pari, A.A.,
957 Gengenbacher, N., *et al.* (2018). Endothelial cell fitness dictates the source of regenerating liver
958 vasculature. J Exp Med *215*, 2497-2508.
959 Snydman, D.R. (2008). The safety of probiotics. Clin Infect Dis *46 Suppl 2*, S104-111; discussion S144-
960 151.
961 Stecher, B., Macpherson, A.J., Hapfelmeier, S., Kremer, M., Stallmach, T., and Hardt, W.D. (2005).
962 Comparison of Salmonella enterica serovar Typhimurium colitis in germfree mice and mice pretreated

963 with streptomycin. Infect Immun *73*, 3228-3241.
964 Stothard, P., and Wishart, D.S. (2005). Circular genome visualization and exploration using CGView.
965 Bioinformatics *21*, 537-539.
966 Tang, Y., Gao, C., Xing, M., Li, Y., Zhu, L., Wang, D., Yang, X., Liu, L., and Yao, P. (2012). Quercetin
967 prevents ethanol-induced dyslipidemia and mitochondrial oxidative damage. Food Chem Toxicol *50*,
968 1194-1200.
969 Tang, Z., Sun, H., Chen, T., Lin, Z., Jiang, H., Zhou, X., Shi, C., Pan, H., Chang, O., Ren, P., *et al.* (2017).
970 Oral delivery of Bacillus subtilis spores expressing cysteine protease of Clonorchis sinensis to grass
971 carp (Ctenopharyngodon idellus): Induces immune responses and has no damage on liver and
972 intestine function. Fish Shellfish Immunol *64*, 287-296.
973 Unban, K., Kochasee, P., Shetty, K., and Khanongnuch, C. (2020). Tannin-Tolerant and Extracellular
974 Tannase Producing Bacillus Isolated from Traditional Fermented Tea Leaves and Their Probiotic
975 Functional Properties. Foods *9*.
976 Wang, L., Gou, X., Ding, Y., Liu, J., Wang, Y., Wang, Y., Zhang, J., Du, L., Peng, W., and Fan, G. (2023). The
977 interplay between herbal medicines and gut microbiota in metabolic diseases. Front Pharmacol *14*,
978 1105405.
979 Wang, Y., Xie, Q., Zhang, Y., Ma, W., Ning, K., Xiang, J.Y., Cui, J., and Xiang, H. (2020). Combination of
980 probiotics with different functions alleviate DSS-induced colitis by regulating intestinal microbiota, IL-
981 10, and barrier function. Appl Microbiol Biotechnol *104*, 335-349.
982 Wu, J., Lin, Z., Wang, X., Zhao, Y., Zhao, J., Liu, H., Johnston, L.J., Lu, L., and Ma, X. (2022).
983 Limosilactobacillus reuteri SLZX19-12 Protects the Colon from Infection by Enhancing Stability of the
984 Gut Microbiota and Barrier Integrity and Reducing Inflammation. Microbiol Spectr *10*, e0212421.
985 Yang, W., Liu, Z., Zhao, Q., Du, H., Yu, J., Wang, H., Liu, X., Liu, H., Jing, X., Yang, H., *et al.* (2022).
986 Population Genetic Structure and Selection Signature Analysis of Beijing Black Pig. Front Genet *13*,
987 860669.
988 Yang, W.H., Westman, J.S., Heithoff, D.M., Sperandio, M., Cho, J.W., Mahan, M.J., and Marth, J.D.
989 (2021). Neu3 neuraminidase induction triggers intestinal inflammation and colitis in a model of
990 recurrent human food-poisoning. Proc Natl Acad Sci U S A *118*.
991 Ye, M., Tang, X., Yang, R., Zhang, H., Li, F., Tao, F., Li, F., and Wang, Z. (2018). Characteristics and
992 Application of a Novel Species of Bacillus: Bacillus velezensis. ACS Chem Biol *13*, 500-505.
993 Zhang, D.X., Kang, Y.H., Zhan, S., Zhao, Z.L., Jin, S.N., Chen, C., Zhang, L., Shen, J.Y., Wang, C.F., Wang,
994 G.Q., *et al.* (2019). Effect of Bacillus velezensis on Aeromonas veronii-Induced Intestinal Mucosal
995 Barrier Function Damage and Inflammation in Crucian Carp (Carassius auratus). Front Microbiol *10*,
996 2663.
997 Zhang, L., Bai, K., Zhang, J., Xu, W., Huang, Q., and Wang, T. (2017). Dietary effects of Bacillus subtilis
998 fmbj on the antioxidant capacity of broilers at an early age. Poult Sci *96*, 3564-3573.
999 Zhang, R., Li, Z., Gu, X., Zhao, J., Guo, T., and Kong, J. (2022). Probiotic Bacillus subtilis LF11 Protects
1000 Intestinal Epithelium Against Salmonella Infection. Front Cell Infect Microbiol *12*, 837886.
1001 Zhou, J., Li, M., Chen, Q., Li, X., Chen, L., Dong, Z., Zhu, W., Yang, Y., Liu, Z., and Chen, Q. (2022).
1002 Programmable probiotics modulate inflammation and gut microbiota for inflammatory bowel disease
1003 treatment after effective oral delivery. Nat Commun *13*, 3432.
1004 Zihni, C., Mills, C., Matter, K., and Balda, M.S. (2016). Tight junctions: from simple barriers to
1005 multifunctional molecular gates. Nat Rev Mol Cell Biol *17*, 564-580.

Figure legends

Fig. 1 Growth curve of *B. velezensis* HBXN2020 and its *in vitro* resistance against environmental assaults. (**A**) Growth curves of *B. velezensis* HBXN2020 cultured in LB medium at 37°C, detection of OD_{600} values at 1 h intervals in microplate reader. (**B**) Survival rate of endospore and vegetative cells of *B. velezensis* HBXN2020 after 30 min at different temperatures (37°C, 45°C, 55°C, 65°C, 75°C, 85°C or 95°C). Equal amounts of endospore and vegetative cells of HBXN2020 were exposed to the following: (**C**) acid solution (pH 2 to 7), (**D**) 0.3% bile salts, (**E**) SGF (pH 1.2) supplemented with pepsin, and (**F**) SIF (pH 6.8) containing trypsin at 37°C. At predetermined time points, 100 μL was taken from each sample, and tenfold serially diluted with sterile PBS (pH 7.2), and then spread on LB agar plates and cultured at 37°C for 12 h before bacterial counting. Each group was repeated three times (n = 3).

Fig. 2 Antibiotic susceptibility of *B. velezensis* HBXN2020 and bacteriostasis assay *in vitro*. (**A**) The diameter of the antibacterial zone indicates the extent of sensitivity to antibiotics. (**B**) The diameter of the antibacterial zone indicates the extent of inhibition against pathogenic bacteria. The diameter of the antibacterial zone was measured with vernier caliper.

Each group was repeated three times (n = 3). R, resistant; I, moderately sensitive; S, sensitive.

Fig. 3 Genomic characteristics and phylogenetic relationships of *B. velezensis* HBXN2020. (**A**) The whole-genome map of *B. velezensis* HBXN2020 with its genomic features. The map consists of 6 circles. From the inner circle to the outer circle: (1) GC-skew, (2) GC content, (3) reverse protein-coding genes, different colors represents different COG functional classifications, (4) genes transcribed in reverse direction, (5) genes transcribed in forward direction, (6) forward protein-coding genes, different colors represents different COG functional classifications. (**B**) The whole genome phylogenetic tree was constructed based on genome-wide data from 14 *bacillus* strains. *B. velezensis* HBXN2020 are indicated in bold.

Fig. 4 *In vivo* safety evaluation of *B. velezensis* HBXN2020 in a mouse model. (**A**) Body weights changes of mice during gavage with *B. velezensis* HBXN2020 spores. Mice were treated with sterile PBS (control group) or low-dose (L-HBXN2020 group), medium dose (M-HBXN2020 group), and high-dose (H-HBXN2020 group) of *B. velezensis* HBXN2020 spores. Weighing and gavage were performed once every two days during the experimental period (15 days). Data were shown as mean values ± SEM (n = 5). (**B**) The mRNA levels of inflammatory cytokines in the colon of mice measured by RT-qPCR.

Data were shown as mean values ± SEM (n = 5). (**C**) The mRNA levels of barrier protein ZO-1, occludin, claudin and Muc2 in the colon of mice measured by RT-qPCR. Data were shown as mean values ± SEM (n = 5). (**D**) Major blood routine parameters and (**E**) serum biochemical parameters of mice in the control group and H-HBXN2020 group. Data were shown as mean values ± SEM (n = 3). (**F**) H&E stained colon sections in the different groups. Scale bar: 200 μm.

Fig. 5 Oral *B. velezensis* HBXN2020 spores alleviated infection by *S.* Typhimurium. (**A**) *In vitro* Bacterial competition between STm and *B. velezensis* HBXN2020. STm were co-incubated with *B. velezensis* HBXN2020 at various ratios at 37°C with shaking. The growth of STm was reflected by bacterial counting per hour. (**B**) Experimental design for treatment in this study. Orally administrated with either sterile PBS, *B. velezensis* HBXN2020 spores or ciprofloxacin by gavage at days 1, 3, and 5 after STm (5×10^7 CFU/mouse) infection, respectively. All mice were euthanized at day 7 after STm infection. (**C**) Bacterial count of STm in mouse feces. Fecal samples were collected per day after STm infection and resuspended in sterile PBS (0.1 g of fecal resuspended in 1 mL of sterile PBS). One hundred microliters of each sample performed a serial of 10-fold dilutions and spread on selective agar plates (50 μg mL^{-1} kanamycin) and incubated at 37°C for 12 h before bacterial counting. The bacterial loads of STm in (**D**) cecum and (**E**) colon.

The cecum and colon were harvested and then homogenized. Statistical signifcance was evaluated using Student's t-test (*, $p < 0.05$, **, $p < 0.01$, and ***, $p < 0.001$). (**F**) Daily body weight changes and (**G**) daily disease activity index (DAI) scores of mice with different treatment groups. Data were shown as mean values ± SEM (n = 6). Statistical signifcance was evaluated using one-way analysis of variance (ANOVA) with Tukey's multiple comparisons test (*, $p < 0.05$, **, $p < 0.01$, and ***, $p < 0.001$). (**H**) Colonic tissue images. (**I**) The length of the colon from per group (n = 6). Statistical signifcance was evaluated using one-way analysis of variance (ANOVA) with Tukey's multiple comparisons test (*, $p < 0.05$, **, $p < 0.01$, and ***, $p < 0.001$).

Fig. 6 Oral *B. velezensis* HBXN2020 spores attenuated colonic damage and inflammatory reaction. (**A**) H&E stained colon tissue sections. Scale bar: 50 μm. The mRNA levels of (**B**) TNF-α, (**C**) IL-1β, (**D**) IL-6, and (**E**) IL-10 were detected by RT-qPCR. Data were shown as mean values ± SEM (n = 5). The mRNA levels of (**F**) ZO-1, (**G**) occludin, (**H**) claudin, and (**I**) Muc2 in colon tissue were detected by RT-qPCR. Data were shown as mean values ± SEM (n = 5). Statistical signifcance was evaluated using one-way analysis of variance (ANOVA) with Tukey's multiple comparisons test (*, $p < 0.05$, **, $p < 0.01$, and ***, $p < 0.001$).

Fig. 7 Oral *B. velezensis* HBXN2020 spores regulated the composition of

intestinal microbiota. The α-diversity of the gut microbiota, determined by the (**A**) Sobs, (**B**) Chao, (**C**) Shannon, and (**D**) Simpson index. Data were shown as mean values ± SEM (n = 5). (**E**) The PCA plot showed the β-diversity of the gut microbiota based on Bray-Curtis distance at the OTU level. Heatmap of the community composition of colonic microbiota at the phylum (top 15 phyla) (**F**) and genus (top 30 genera) (**G**) level. Relative abundance of selected taxa (**H**) *norank_f_Muribaculaceae*, (**I**) *Lactobacillus*, (**J**) *Akkermansia*, and (**K**) *Enterococcus*. (**L**) Analysis of differences in the microbial communities by LEfSe (linear discriminant analysis, LDA score > 2) among different groups. Signifcance was evaluated by one-way analysis of variance (ANOVA) with Tukey's multiple comparisons test (*, $p < 0.05$, **, $p < 0.01$, and ***, $p < 0.001$).

Fig. 8 Prophylactic *B. velezensis* HBXN2020 spores attenuated the symptoms of *S.* Typhimurium-infected mouse. (**A**) Experimental design for treatment in this study. At days 1, 3, 5, and 7, each mouse in the HBXN2020+STm group, CIP+STm group, and PBS+STm group were received 200 μL of *B. velezensis* HBXN2020 spores (1×10^8 CFU/mouse), ciprofloxacin or sterile PBS by gavage, respectively. Then, mice in PBS+STm group, HBXN2020+STm group and CIP+STm group were orally inoculated with 200 μL (5×10^7 CFU/mouse) of STm on day 7, respectively. On day 12, all mice were euthanized. (**B**) Daily body weight changes and (**C**) daily disease

activity index (DAI) scores of mice with different groups following STm treatment. Data were shown as mean values ± SEM (n = 6). Statistical signifcance was evaluated using one-way analysis of variance (ANOVA) with Tukey's multiple comparisons test (*, $p < 0.05$, **, $p < 0.01$, and ***, $p < 0.001$). (**D**) Colonic tissue images. (**E**) The length of the colon from per group (n = 6). (**F**) Bacterial count of STm in mouse feces. Fecal samples were collected every day after STm infection and resuspended in sterile PBS (0.1 g of fecal resuspended in 1 mL of sterile PBS). One hundred microliters of each sample performed a serial of 10-fold dilutions and spread on selective agar plates (50 μg mL^{-1} kanamycin) and incubated at 37°C for 12 h before bacterial counting. The bacterial loads of STm in (**G**) cecum and (**H**) colon. The cecum and colon were harvested and then homogenized. Statistical signifcance was evaluated using Student's t-test (*, $p < 0.05$, **, $p < 0.01$, and ***, $p < 0.001$).

Fig. 9 Prophylactic *B. velezensis* HBXN2020 spores attenuated colonic damage and inflammatory reaction. (**A**) H&E stained colon tissue sections. Scale bar: 50 μm. The mRNA levels of (**B**) TNF-α, (**C**) IL-1β, (**D**) IL-6, and (**E**) IL-10 were detected by RT-qPCR. Data were shown as mean values ± SEM (n = 5). The mRNA levels of (**F**) ZO-1, (**G**) occludin, (**H**) claudin, and (**I**) Muc2 in colon tissue were detected by RT-qPCR. Data were shown as mean values ± SEM (n = 6). Statistical signifcance was evaluated using one-way analysis of variance (ANOVA) with Tukey's multiple comparisons test (*, $p < 0.05$, **, p

< 0.01, and ***, $p < 0.001$).

Fig. 10 Prophylactic *B. velezensis* HBXN2020 spores regulated the composition of gut microbiota. (**A** to **D**) Alpha diversity of the intestinal microbiota. Data were shown as mean values ± SEM (n = 5). (**E**) The PCA plot showed the β-diversity among different microbial community groups based on Bray-Curtis distance at the OTU level. Heatmap of the community composition of colonic microbiota at the phylum (top 15 phyla) (**F**) and genus (top 30 genera) (**G**) level. Relative abundance of selected taxa (**H**) *Lactobacillus*, (**I**) *Akkermansia*, (**J**) *Alistipes*, (**K**) *Bacteroides*, (**L**) *Escherichia-Shigella*, and (**M**) *Enterococcus*. Data were shown as mean values ± SEM (n = 5). (**N**) Analysis of differences in the microbial taxa by LEfSe (LDA score > 2) in different groups. Signifcance was evaluated by one-way analysis of variance (ANOVA) with Tukey's multiple comparisons test (*, $p < 0.05$, **, $p < 0.01$, and ***, $p < 0.001$).

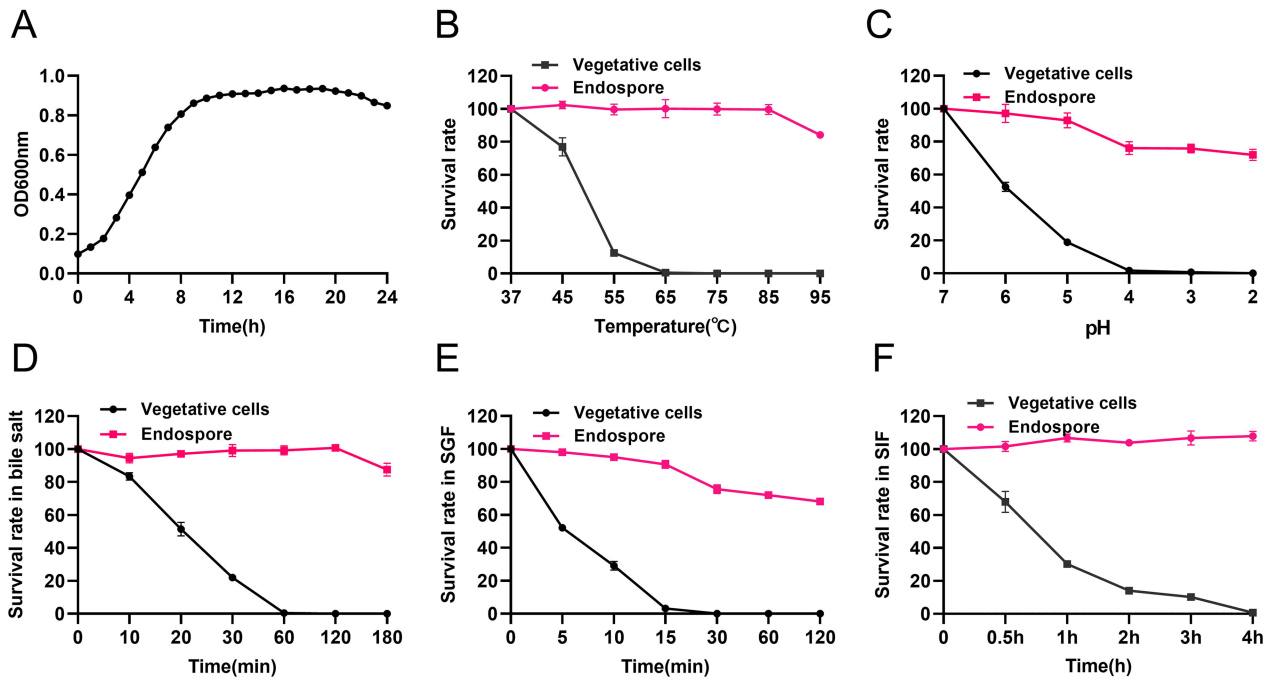
A
OD600nm
1.0
0.8
0.6
0.4
0.2
0.0
0
4
8
12
16
20
24
Time(h)
B
Vegetative cells
Endospore
Survival rate
120
100
80
60
40
20
0
37
45
55
65
75
85
95
Temperature(℃)
C
Vegetative cells
Endospore
Survival rate
120
100
80
60
40
20
0
7
6
5
4
3
2
pH
D
Vegetative cells
Endospore
Survival rate in bile salt
120
100
80
60
40
20
0
0
10
20
30
60
120
180
Time(min)
E
Vegetative cells
Endospore
Survival rate in SGF
120
100
80
60
40
20
0
0
5
10
15
30
60
120
Time(min)
F
Vegetative cells
Endospore
Survival rate in SIF
120
100
80
60
40
20
0
0
0.5h
1h
2h
3h
4h
Time(h)

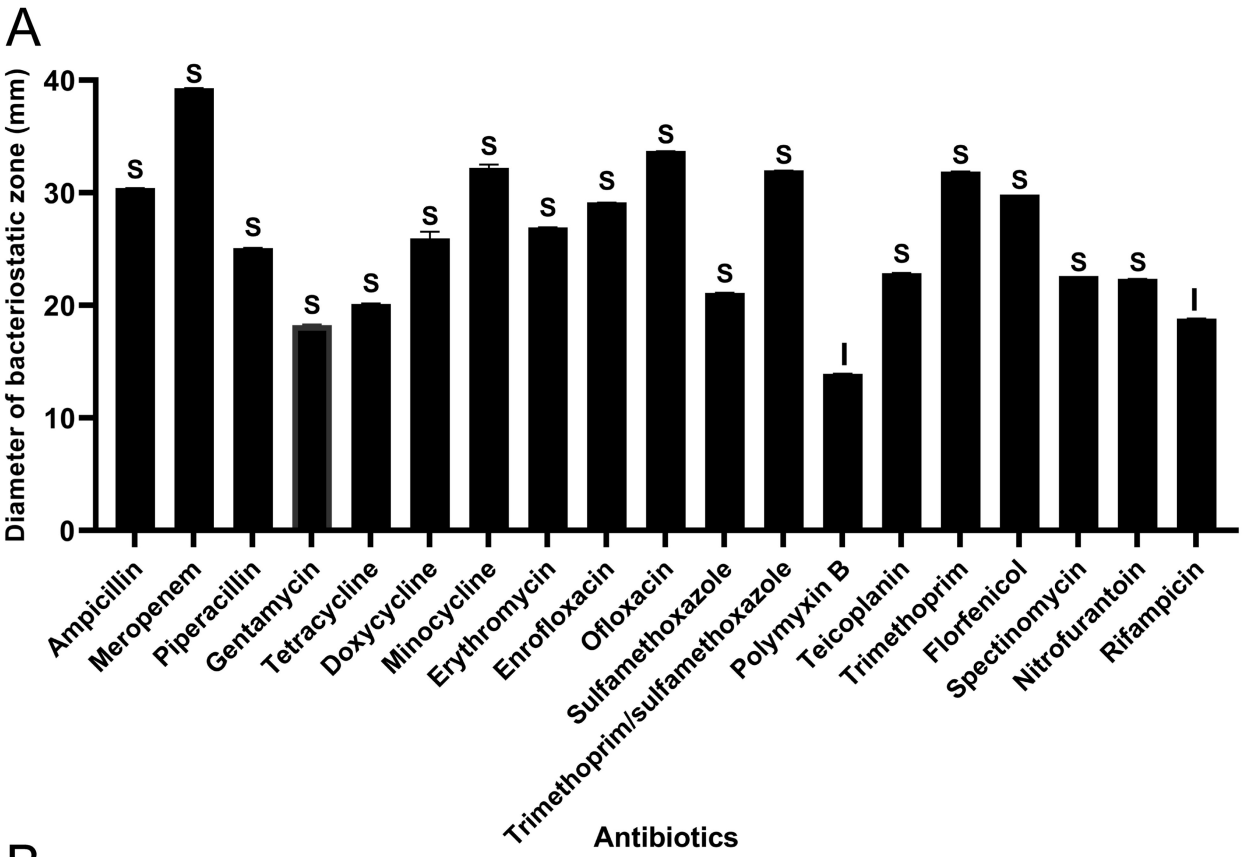
A
Diameter of bacteriostatic zone (mm)
0
10
20
30
40
S
S
S
S
S
S
S
S
S
S
S
I
S
S
S
S
S
I
Ampicillin
Meropenem
Piperacillin
Gentamycin
Tetracycline
Doxycycline
Minocycline
Erythromycin
Enrofloxacin
Ofloxacin
Sulfamethoxazole
Trimethoprim/sulfamethoxazole
Polymyxin B
Teicoplanin
Trimethoprim
Florfenicol
Spectinomycin
Nitrofurantoin
Rifampicin
Antibiotics

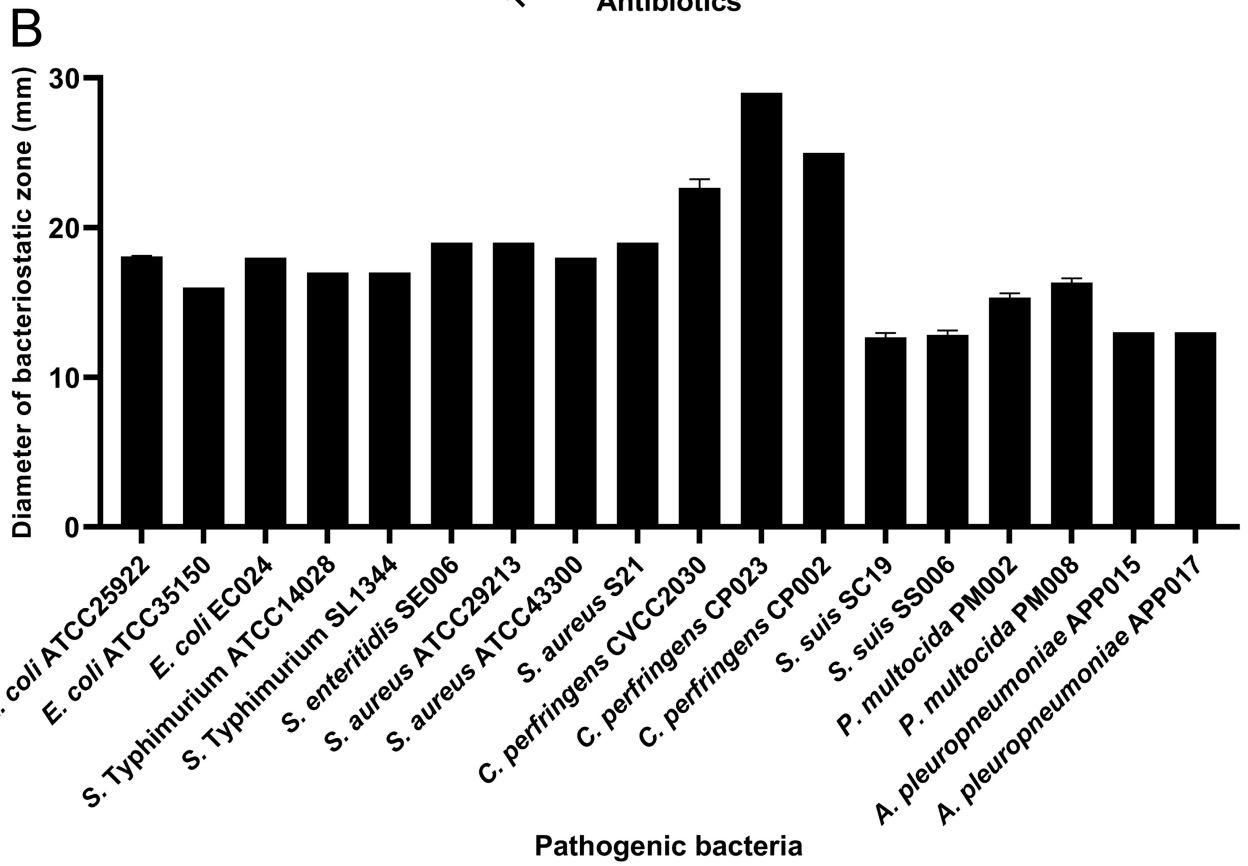
B
Diameter of bacteriostatic zone (mm)
0
10
20
30
E. coli ATCC25922
E. coli ATCC35150
E. coli EC024
S. Typhimurium ATCC14028
S. Typhimurium SL1344
S. enteritidis SE006
S. aureus ATCC29213
S. aureus ATCC43300
S. aureus S21
C. perfringens CVCC2030
C. perfringens CP023
C. perfringens CP002
S. suis SC19
S. suis SS006
P. multocida PM002
P. multocida PM008
A. pleuropneumoniae APP015
A. pleuropneumoniae APP017
Pathogenic bacteria

A

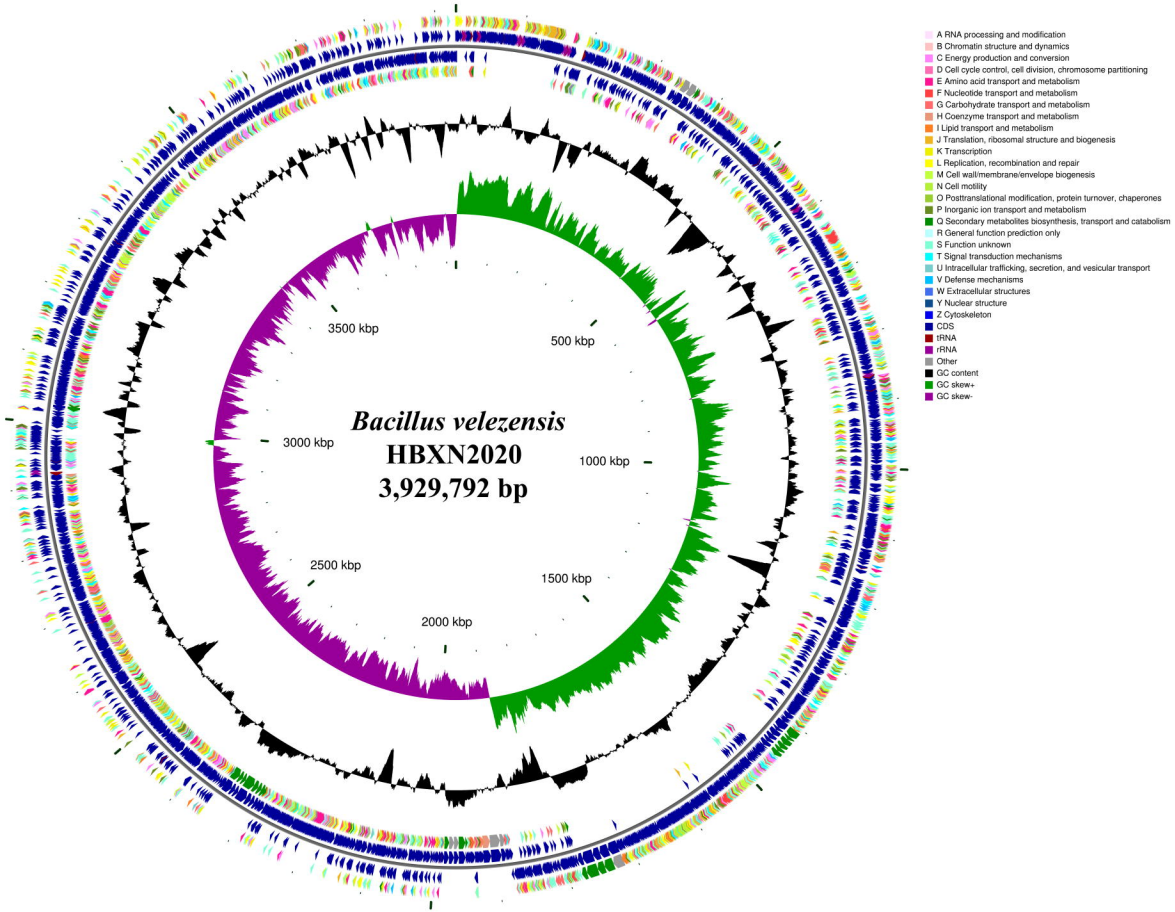
A RNA processing and modification
B Chromatin structure and dynamics
C Energy production and conversion
D Cell cycle control, cell division, chromosome partitioning
E Amino acid transport and metabolism
F Nucleotide transport and metabolism
G Carbohydrate transport and metabolism
H Coenzyme transport and metabolism
I Lipid transport and metabolism
J Translation, ribosomal structure and biogenesis
K Transcription
L Replication, recombination and repair
M Cell wall/membrane/envelope biogenesis
N Cell motility
O Posttranslational modification, protein turnover, chaperones
P Inorganic ion transport and metabolism
Q Secondary metabolites biosynthesis, transport and catabolism
R General function prediction only
S Function unknown
T Signal transduction mechanisms
U Intracellular trafficking, secretion, and vesicular transport
V Defense mechanisms
W Extracellular structures
Y Nuclear structure
Z Cytoskeleton
CDS
tRNA
rRNA
Other
GC content
GC skew+
GC skew-
3500 kbp
500 kbp
Bacillus velezensis
HBXN2020
3,929,792 bp
3000 kbp
1000 kbp
2500 kbp
1500 kbp
2000 kbp

B

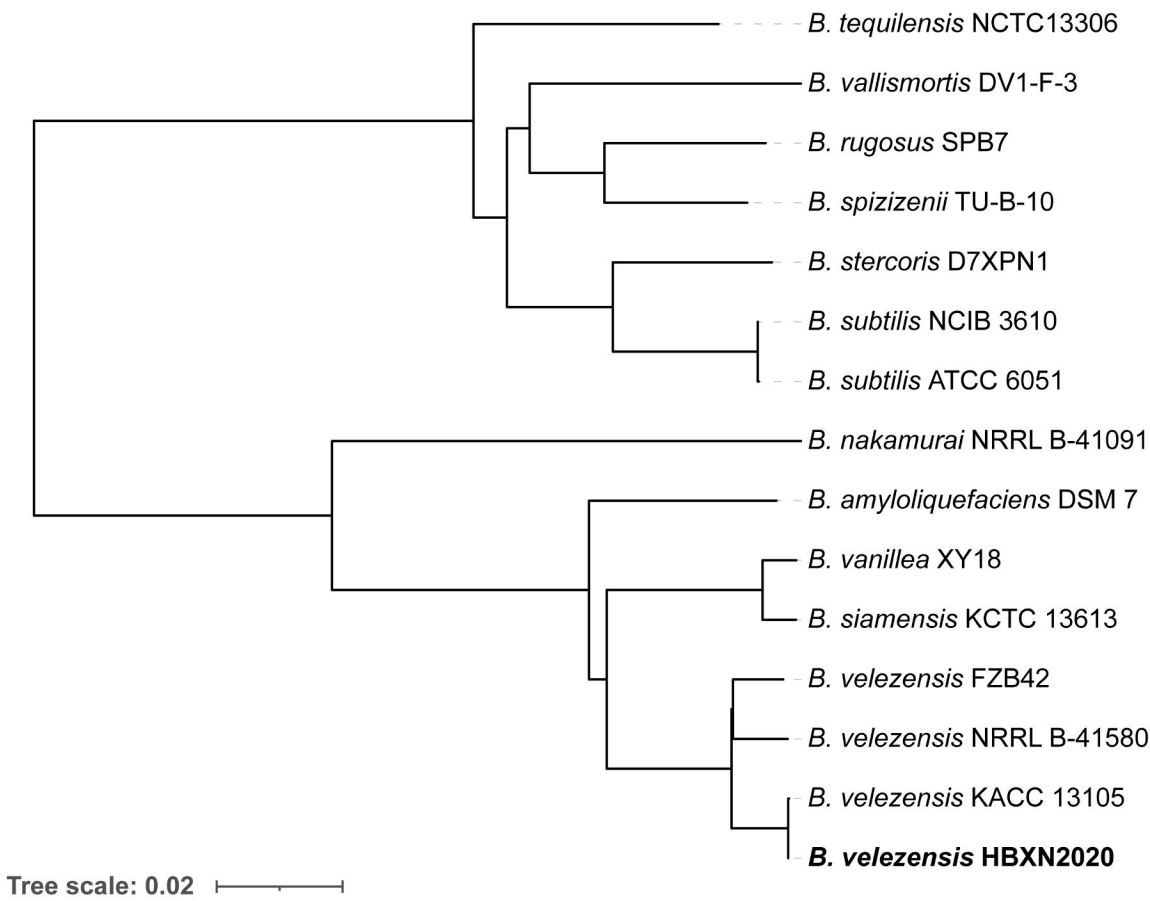
B. tequilensis NCTC13306
B. vallismortis DV1-F-3
B. rugosus SPB7
B. spizizenii TU-B-10
B. stercoris D7XPN1
B. subtilis NCIB 3610
B. subtilis ATCC 6051
B. nakamurai NRRL B-41091
B. amyloliquefaciens DSM 7
B. vanillea XY18
B. siamensis KCTC 13613
B. velezensis FZB42
B. velezensis NRRL B-41580
B. velezensis KACC 13105
B. velezensis HBXN2020
Tree scale: 0.02

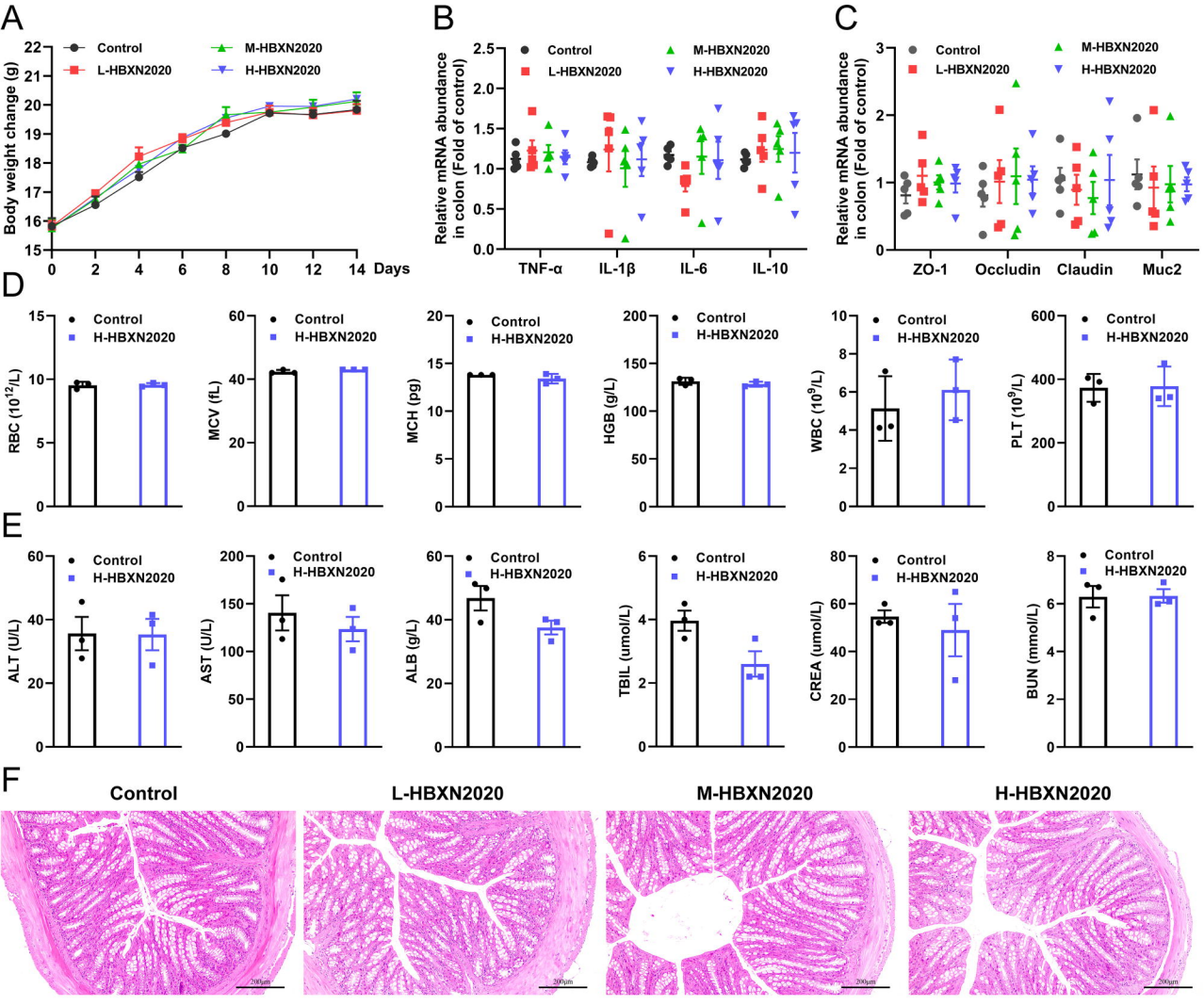
A
Control
L-HBXN2020
M-HBXN2020
H-HBXN2020
Body weight change (g)
Days
B
Relative mRNA abundance in colon (Fold of control)
TNF-α
IL-1β
IL-6
IL-10
C
ZO-1
Occludin
Claudin
Muc2
D
RBC (10^{12}/L)
MCV (fL)
MCH (pg)
HGB (g/L)
WBC (10^9/L)
PLT (10^9/L)
E
ALT (U/L)
AST (U/L)
ALB (g/L)
TBIL (umol/L)
CREA (umol/L)
BUN (mmol/L)
F
Control
L-HBXN2020
M-HBXN2020
H-HBXN2020

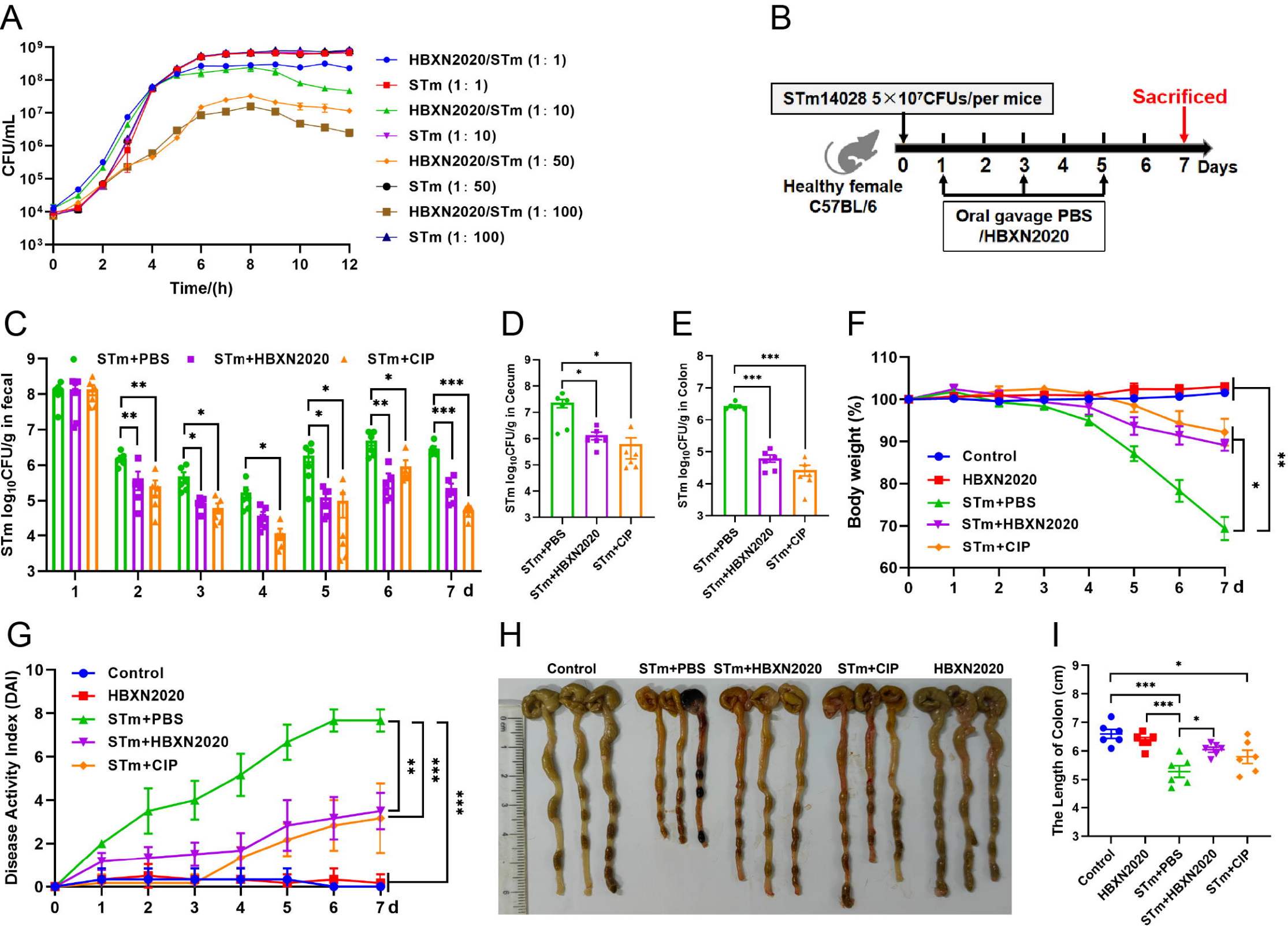
A
CFU/mL
Time/(h)
HBXN2020/STm (1：1)
STm (1：1)
HBXN2020/STm (1：10)
STm (1：10)
HBXN2020/STm (1：50)
STm (1：50)
HBXN2020/STm (1：100)
STm (1：100)
B
STm14028 5×10⁷CFUs/per mice
Sacrificed
Healthy female C57BL/6
Days
Oral gavage PBS /HBXN2020
C
STm+PBS
STm+HBXN2020
STm+CIP
STm log10CFU/g in fecal
d
D
STm log10CFU/g in Cecum
E
STm log10CFU/g in Colon
F
Body weight (%)
Control
HBXN2020
STm+PBS
STm+HBXN2020
STm+CIP
G
Disease Activity Index (DAI)
H
Control
STm+PBS
STm+HBXN2020
STm+CIP
HBXN2020
I
The Length of Colon (cm)

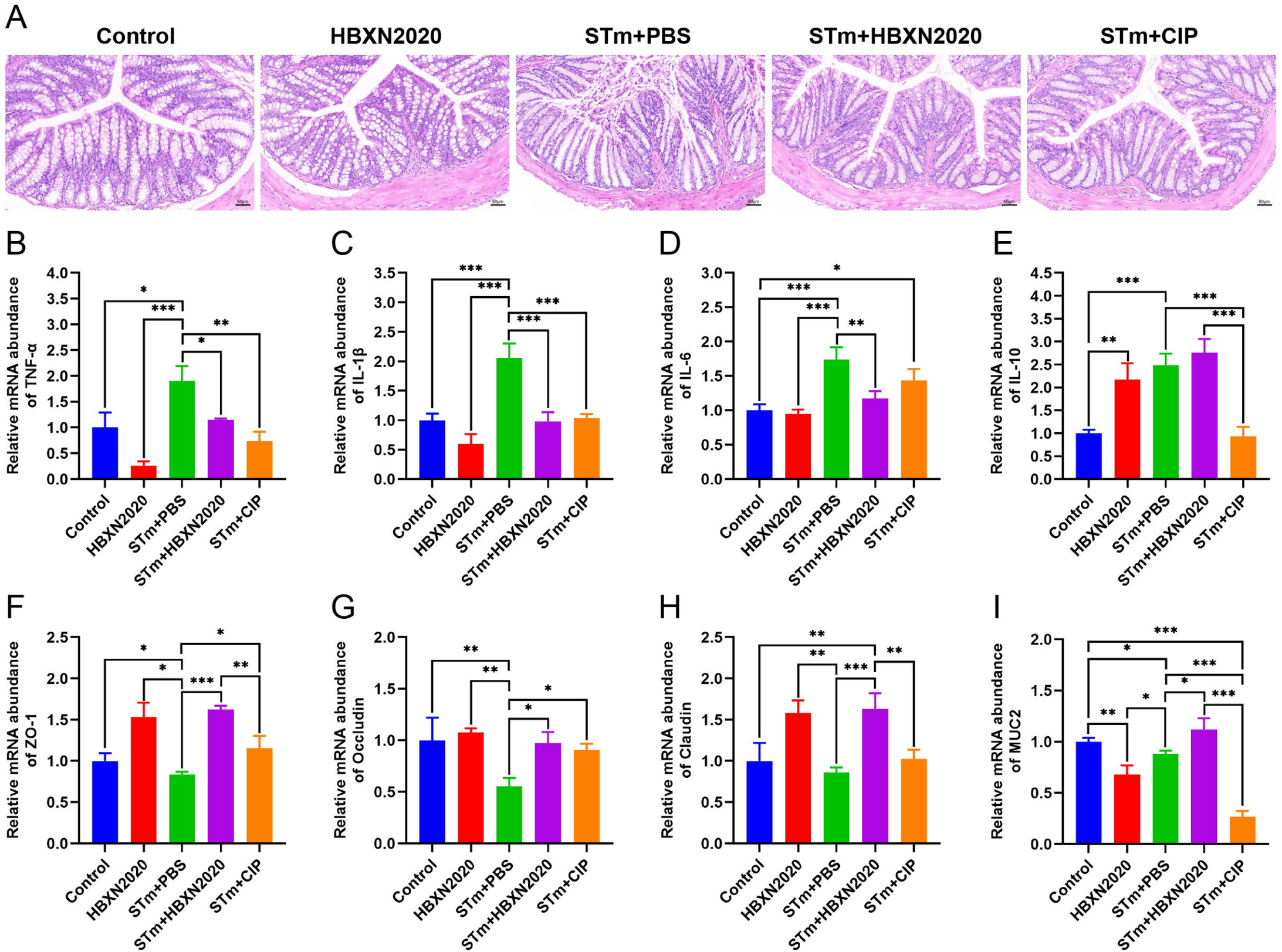
A
Control
HBXN2020
STm+PBS
STm+HBXN2020
STm+CIP
B
Relative mRNA abundance of TNF-α
C
Relative mRNA abundance of IL-1β
D
Relative mRNA abundance of IL-6
E
Relative mRNA abundance of IL-10
F
Relative mRNA abundance of ZO-1
G
Relative mRNA abundance of Occludin
H
Relative mRNA abundance of Claudin
I
Relative mRNA abundance of MUC2
Control
HBXN2020
STm+PBS
STm+HBXN2020
STm+CIP

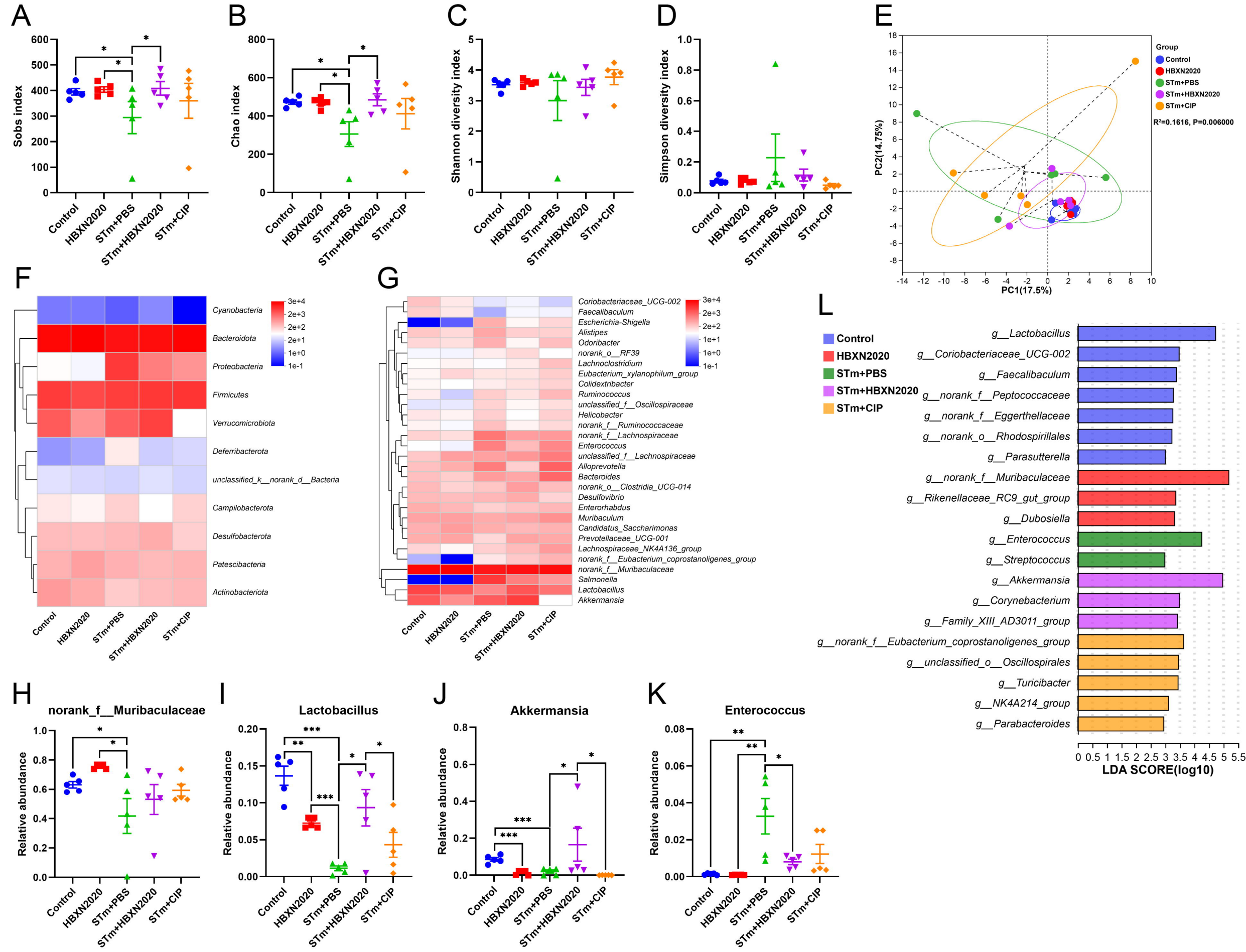
A
Sobs index
B
Chao index
C
Shannon diversity index
D
Simpson diversity index
Control
HBXN2020
STm+PBS
STm+HBXN2020
STm+CIP
E
Group
Control
HBXN2020
STm+PBS
STm+HBXN2020
STm+CIP
R²=0.1616, P=0.006000
PC2(14.75%)
PC1(17.5%)
F
Cyanobacteria
Bacteroidota
Proteobacteria
Firmicutes
Verrucomicrobiota
Deferribacterota
unclassified_k__norank_d__Bacteria
Campilobacterota
Desulfobacterota
Patescibacteria
Actinobacteriota
G
Coriobacteriaceae_UCG-002
Faecalibaculum
Escherichia-Shigella
Alistipes
Odoribacter
norank_o__RF39
Lachnoclostridium
Eubacterium_xylanophilum_group
Colidextribacter
Ruminococcus
unclassified_f__Oscillospiraceae
Helicobacter
norank_f__Ruminococcaceae
norank_f__Lachnospiraceae
Enterococcus
unclassified_f__Lachnospiraceae
Alloprevotella
Bacteroides
norank_o__Clostridia_UCG-014
Desulfovibrio
Enterorhabdus
Muribaculum
Candidatus_Saccharimonas
Prevotellaceae_UCG-001
Lachnospiraceae_NK4A136_group
norank_f__Eubacterium_coprostanoligenes_group
norank_f__Muribaculaceae
Salmonella
Lactobacillus
Akkermansia
L
Control
HBXN2020
STm+PBS
STm+HBXN2020
STm+CIP
g__Lactobacillus
g__Coriobacteriaceae_UCG-002
g__Faecalibaculum
g__norank_f__Peptococcaceae
g__norank_f__Eggerthellaceae
g__norank_o__Rhodospirillales
g__Parasutterella
g__norank_f__Muribaculaceae
g__Rikenellaceae_RC9_gut_group
g__Dubosiella
g__Enterococcus
g__Streptococcus
g__Akkermansia
g__Corynebacterium
g__Family_XIII_AD3011_group
g__norank_f__Eubacterium_coprostanoligenes_group
g__unclassified_o__Oscillospirales
g__Turicibacter
g__NK4A214_group
g__Parabacteroides
LDA SCORE(log10)
H
norank_f__Muribaculaceae
I
Lactobacillus
J
Akkermansia
K
Enterococcus
Relative abundance

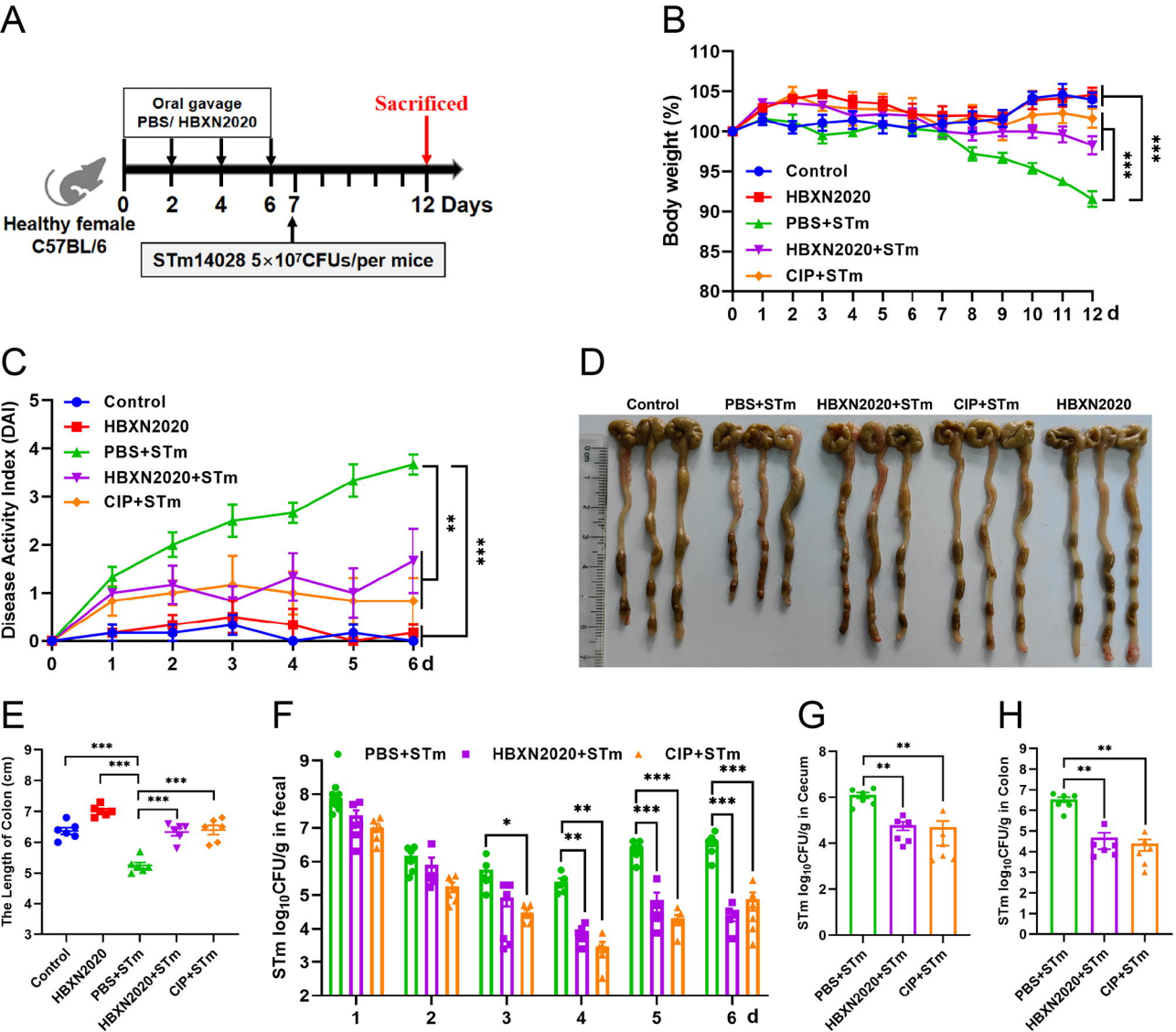
A
Oral gavage
PBS/ HBXN2020
Sacrificed
Healthy female
C57BL/6
0
2
4
6
7
12 Days
STm14028 5×10⁷CFUs/per mice
B
Body weight (%)
Control
HBXN2020
PBS+STm
HBXN2020+STm
CIP+STm
d
C
Disease Activity Index (DAI)
Control
HBXN2020
PBS+STm
HBXN2020+STm
CIP+STm
d
D
Control
PBS+STm
HBXN2020+STm
CIP+STm
HBXN2020
E
The Length of Colon (cm)
Control
HBXN2020
PBS+STm
HBXN2020+STm
CIP+STm
F
PBS+STm
HBXN2020+STm
CIP+STm
STm log10CFU/g in fecal
d
G
STm log10CFU/g in Cecum
PBS+STm
HBXN2020+STm
CIP+STm
H
STm log10CFU/g in Colon
PBS+STm
HBXN2020+STm
CIP+STm

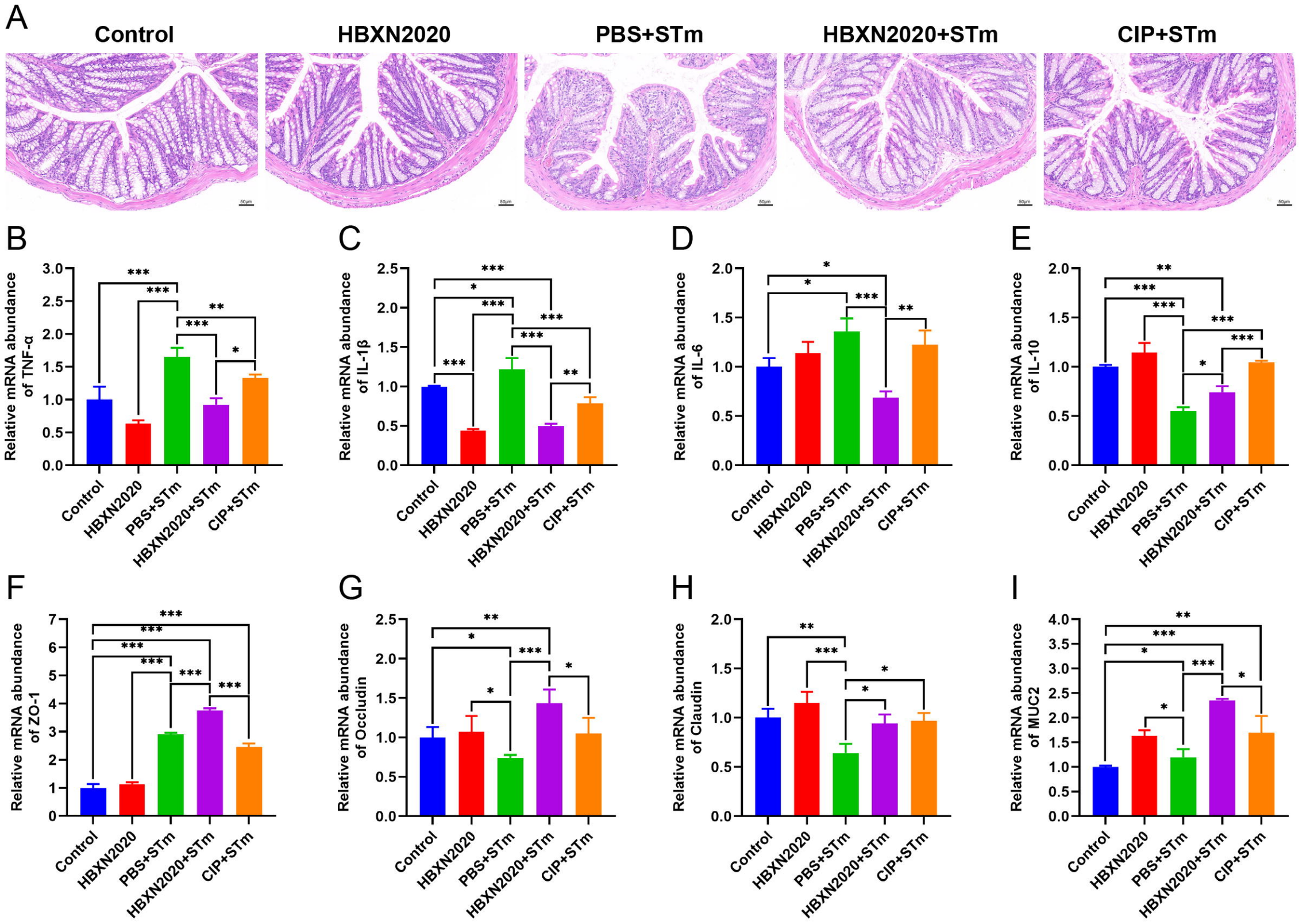
A
Control
HBXN2020
PBS+STm
HBXN2020+STm
CIP+STm
B
Relative mRNA abundance of TNF-α
C
Relative mRNA abundance of IL-1β
D
Relative mRNA abundance of IL-6
E
Relative mRNA abundance of IL-10
F
Relative mRNA abundance of ZO-1
G
Relative mRNA abundance of Occludin
H
Relative mRNA abundance of Claudin
I
Relative mRNA abundance of MUC2
Control
HBXN2020
PBS+STm
HBXN2020+STm
CIP+STm

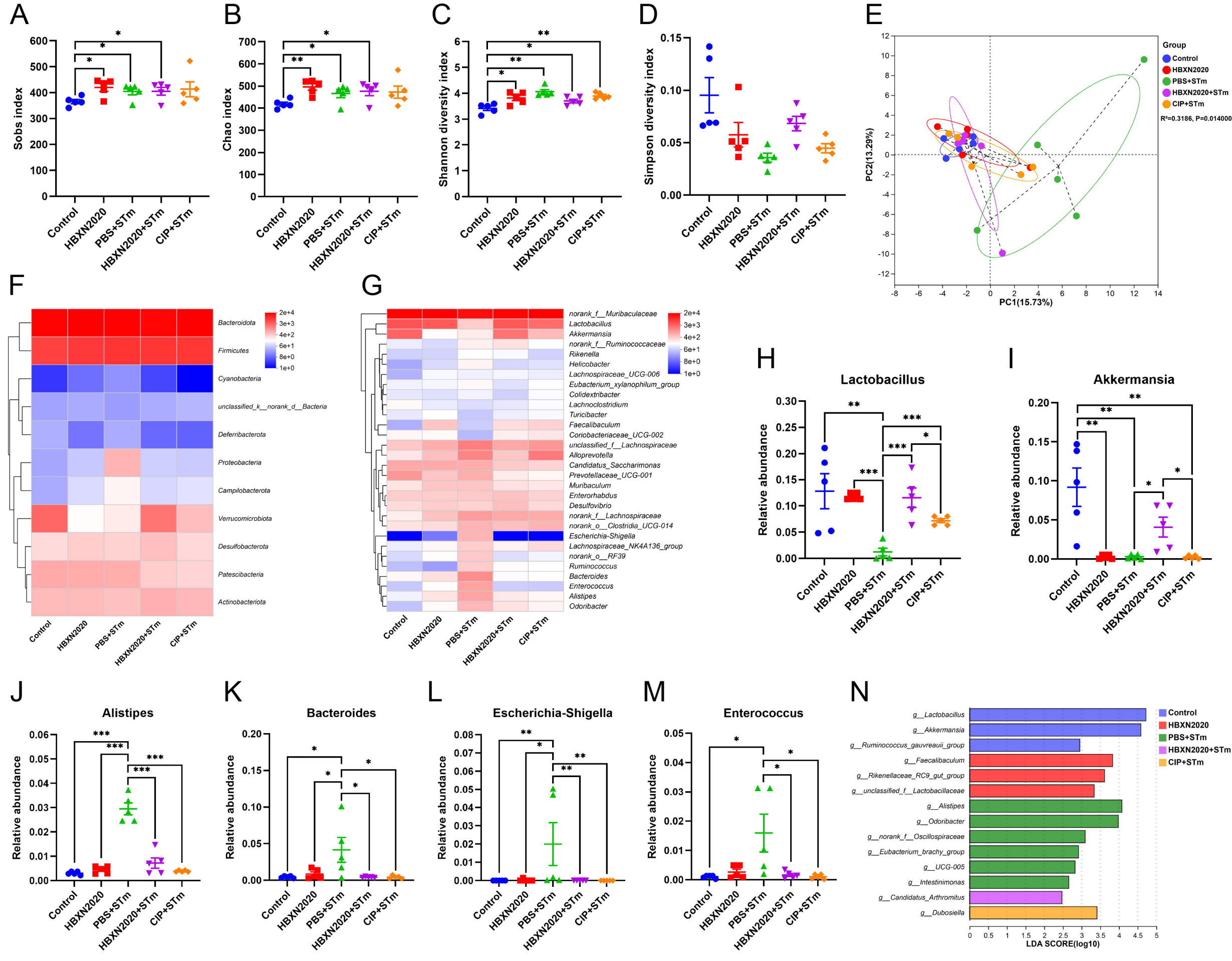
A
Sobs index
B
Chao index
C
Shannon diversity index
D
Simpson diversity index
Control
HBXN2020
PBS+STm
HBXN2020+STm
CIP+STm
E
Group
Control
HBXN2020
PBS+STm
HBXN2020+STm
CIP+STm
R²=0.3186, P=0.014000
PC2(13.29%)
PC1(15.73%)
F
Bacteroidota
Firmicutes
Cyanobacteria
unclassified_k__norank_d__Bacteria
Deferribacterota
Proteobacteria
Campilobacterota
Verrucomicrobiota
Desulfobacterota
Patescibacteria
Actinobacteriota
G
norank_f__Muribaculaceae
Lactobacillus
Akkermansia
norank_f__Ruminococcaceae
Rikenella
Helicobacter
Lachnospiraceae_UCG-006
Eubacterium_xylanophilum_group
Colidextribacter
Lachnoclostridium
Turicibacter
Faecalibaculum
Coriobacteriaceae_UCG-002
unclassified_f__Lachnospiraceae
Alloprevotella
Candidatus_Saccharimonas
Prevotellaceae_UCG-001
Muribaculum
Enterorhabdus
Desulfovibrio
norank_f__Lachnospiraceae
norank_o__Clostridia_UCG-014
Escherichia-Shigella
Lachnospiraceae_NK4A136_group
norank_o__RF39
Ruminococcus
Bacteroides
Enterococcus
Alistipes
Odoribacter
H
Lactobacillus
Relative abundance
I
Akkermansia
J
Alistipes
K
Bacteroides
L
Escherichia-Shigella
M
Enterococcus
N
g__Lactobacillus
g__Akkermansia
g__Ruminococcus_gauvreauii_group
g__Faecalibaculum
g__Rikenellaceae_RC9_gut_group
g__unclassified_f__Lactobacillaceae
g__Alistipes
g__Odoribacter
g__norank_f__Oscillospiraceae
g__Eubacterium_brachy_group
g__UCG-005
g__Intestinimonas
g__Candidatus_Arthromitus
g__Dubosiella
LDA SCORE(log10)